

UNCLASSIFIED

AD NUMBER

ADB004732

LIMITATION CHANGES

TO:

Approved for public release; distribution is unlimited.

FROM:

Distribution authorized to U.S. Gov't. agencies only; Administrative/Operational Use; MAR 1975. Other requests shall be referred to Federal Aviation Administration, Supersonic Transport Office, 800 Independence Avenue, SW, Washington, DC 20590. This document contains export-controlled technical data.

AUTHORITY

faa ltr, 26 apr 1977

THIS PAGE IS UNCLASSIFIED


THIS REPORT HAS BEEN DELIMITED  
AND CLEARED FOR PUBLIC RELEASE  
UNDER DOD DIRECTIVE 5200.20 AND  
NO RESTRICTIONS ARE IMPOSED UPON  
ITS USE AND DISCLOSURE.

DISTRIBUTION STATEMENT A

APPROVED FOR PUBLIC RELEASE;  
DISTRIBUTION UNLIMITED.

②

AD B 0 0 4 7 3 2

AD No.  FILE COPY  
DDC

**SST Technology**  
**Follow-On Program—Phase II**  
**NOISE SUPPRESSOR/NOZZLE DEVELOPMENT**  
**VOLUME V**

**PERFORMANCE TECHNOLOGY—THE EFFECT OF  
INITIAL JET CONDITIONS ON THE MIXING  
AND PERFORMANCE OF A 2-D CONSTANT AREA EJECTOR**

**R. L. Thornock, R. S. Armstrong**

**Boeing Commercial Airplane Company**

**P.O. Box 3707**

**Seattle, Washington 98124**



**D6-41487**

**March 1975**

**FINAL REPORT**

**Task III**

Approved for U.S. Government only. This document is exempted from public availability because of restrictions imposed by the Export Control Act. Transmittal of this document outside the U.S. Government must have prior approval of the Supersonic Transport Office.

**Prepared for**  
**FEDERAL AVIATION ADMINISTRATION**  
**Supersonic Transport Office**  
**800 Independence Avenue, S.W.**  
**Washington, D.C. 20590**

**DDC**  
**RECEIVED**  
**JUN 27 1975**  


The contents of this report reflect the views of the Boeing Commercial Airplane Company, which is responsible for the facts and the accuracy of the data presented herein. The contents do not necessarily reflect the official views or policy of the Department of Transportation. This report does not constitute a standard, specification, or regulation.

DISTRIBUTION TO	
NTIS	DOT <input checked="" type="checkbox"/>
DDC	DOT <input checked="" type="checkbox"/>
REMARKS	
JUSTIFICATION	
BY	
DISTRIBUTION / RELEVANCE / DATE	
DATE	
13	



TECHNICAL REPORT STANDARD TITLE PAGE

1. Report No. FAA-SS-73-11-5	2. Government Accession No.	3. Recipient's Catalog No. 12 657
4. Title and Subtitle SST Technology Follow-On Program-Phase II Noise Suppressor/Nozzle Development, Volume V, Performance Technology-The Effect of Initial Jet Conditions on a 2-D Constant Area Ejector		5. Report Date Mar 1975
6. Performing Organization Code		7. Author(s) R. L. Thornock R. S. Armstrong
8. Performing Organization Report No. D6-41487		9. Performing Organization Name and Address Boeing Commercial Airplane Company P.O. Box 3707 Seattle, Washington 98124
10. Work Unit No.		11. Contract or Grant No. DOT-FA-72WA-2893
12. Sponsoring Agency Name and Address Federal Aviation Administration, Supersonic Transport Office 800 Independence Avenue S. W. Washington, D.C. 20590		13. Type of Report and Period Covered Final Report, Task III
14. Sponsoring Agency Code		15. Supplementary Notes S. Blatt, DOT/SST Technical Monitor
16. Abstract The effects of initial jet conditions on the performance and mixing in a constant area ejector were investigated. Initial jet conditions varied with velocity profile, base thickness, and primary turbulence level. An effect of each of these quantities on thrust and weight flow augmentation was noted. Profile measurements were affected substantially by ejector wall boundary layer growth and could not be used. Spark shadowgraphs, made through the clear ejector sidewalls, show noticeable effects of initial conditions at high pressure ratios.  6 SST Technology Follow-On Program-Phase II. Noise Suppressor/Nozzle Development. Volume V. Performance Technology-The Effect of Initial Jet Conditions on the Mixing and Performance of a 2-D Constant Area Ejector.		
17. Key Words Supersonic transport Velocity profile Suppressor nozzle Base thickness Ejector performance Turbulence level Flow visualization Initial conditions		18. Distribution Statement Approved for U.S. Government only. This document is exempted from public availability because of restrictions imposed by the Export Control Act. Transmittal of this document outside the U.S. Government must have prior approval of the Supersonic Transport Office.
19. Security Classif. (of this report)	20. Security Classif. (of this page)	21. No. of Pages 59
		22. Price

## PREFACE

This is one of a series of final reports on noise and propulsion technology submitted by the Boeing Commercial Airplane Company, Seattle, Washington, 98124, in fulfillment of Task III of Department of Transportation Contract DOT-FA-72WA-2803, dated 1 February 1972.

To benefit utilization of technical data developed by the noise suppressor and nozzle development program, the final report is divided into 10 volumes covering key technology areas and a summary of total program results. The 10 volumes are issued under the master title, "Noise Suppressor/Nozzle Development." Detailed volume breakdown is as follows:

		Report No.
Volume I	— Program Summary	FAA-SS-73-11-1
Volume II	— Noise Technology	FAA-SS-73-11-2
Volume III	— Noise Technology—Backup Data Report	FAA-SS-73-11-3
Volume IV	— Performance Technology Summary	FAA-SS-73-11-4
Volume V	— Performance Technology—The Effect of Initial Jet Conditions on a 2-D Constant Area Ejector	FAA-SS-73-11-5
Volume VI	— Performance Technology—Thrust and Flow Characteristics of a Reference Multitube Nozzle With Ejector	FAA-SS-73-11-6
Volume VII	— Performance Technology—A Guide to Multitube Suppressor Nozzle Static Performance: Trends and Trades	FAA-SS-73-11-7
Volume VIII	— Performance Technology—Multitube Suppressor/Ejector Interaction Effects on Static Performance (Ambient and 1150° F Jet Temperature)	FAA-SS-73-11-8
Volume IX	— Performance Technology—Analysis of the Low-Speed Performance of Multitube Suppressor/Ejector Nozzles (0-167 kn)	FAA-SS-73-11-9
Volume X	— Advanced Suppressor Concepts and Full-Scale Tests	FAA-SS-73-11-10

This report is volume V of the series and was prepared by the Propulsion Research Staff of the Boeing Commercial Airplane Company.

PRECEDING PAGE BLANK-NOT FILMED

## SUMMARY

The effects of initial flow characteristics (velocity profile, turbulence level, and initial base thickness) on ejector performance have often been ignored in test planning. Because these quantities can possibly affect the mixing process inside the ejector, they might also have an effect on the overall ejector performance. While model and full-scale ejector nozzles may be geometrically similar, their initial flow characteristics at the beginning of mixing may differ greatly, introducing uncertainties into the prediction of full-scale performance from model-scale data.

Accordingly, a test program was carried out to observe the effect, if any, of these variables on thrust augmentation, pumping, and mixing of ejectors typically considered as noise suppressors for SST applications. An ejector apparatus was fabricated for use on the Boeing high ratio rig, consisting of an array of slot nozzles exhausting into a mixing section of rectangular cross section. The two long sides of this section were of clear plastic to permit spark shadowgraph photos to be taken. Both primary and secondary flows were metered, and they entered the mixing section through the nozzle assembly as substantially uniform and parallel flows.

A baseline nozzle configuration was tested, and then one variation each was done of initial mean velocity profile, turbulence intensity, and base thickness while holding the other two variables fixed. The velocity profile variation was accomplished by lengthening the nozzle throat by 12 nozzle heights (6 in.) in a constant area section, producing a larger initial boundary layer thickness. Turbulence intensity was varied by inserting upstream blockages in the primary flow. Base thickness was varied by chamfering the downstream end of the plate separating primary and secondary flows.

The effects of the three variations in initial conditions on augmentation and weight flow ratio are shown in figures 1 and 2, respectively. Both the thick base and long throat configuration display lower performance than the baseline throughout all or part of the pressure ratio range. The performance of the high primary turbulence variation, on the other hand, is slightly higher throughout the range of pressure ratios tested. Spark shadowgraph photos of the baseline configuration are shown in figure 3 for a series of pressure ratios. Of particular interest is the contrast between subsonic ( $P_{Tp}/P_{amb} < 3.0$ ) and supersonic ( $P_{Tp}/P_{amb} \geq 3.5$ ) flow regimes. In the latter case, comparatively uniform primary flows are apparent with only a weak oblique shock structure.

It is concluded that:

1. Each of the test variations produced a noticeable change in ejector performance. For this reason, the effects of initial flow conditions should be accounted for when estimating the performance of ejector nozzles.
2. Because of the apparent uniformity of the flow in the supersonic mode of ejector operation, it apparently can be adequately modeled by analyses which neglect transverse pressure gradients.

PRECEDING PAGE BLANK NOT FILMED

## CONTENTS

	Page
1.0 INTRODUCTION . . . . .	1
2.0 TEST DESCRIPTION . . . . .	3
2.1 Range of Variables . . . . .	3
2.2 Test Hardware . . . . .	4
2.3 Instrumentation . . . . .	5
2.4 Test Procedure . . . . .	5
3.0 TEST RESULTS . . . . .	7
3.1 Baseline Calibration . . . . .	7
3.2 Baseline Performance . . . . .	7
3.3 Long Throat Configuration . . . . .	8
3.4 Thick Base Configuration Performance . . . . .	9
3.5 High Primary Turbulence Performance . . . . .	9
3.6 Comparison With 1-D Ejector Theory . . . . .	10
3.7 Mixing Profiles and Static Pressure Distributions . . . . .	11
4.0 CONCLUSIONS . . . . .	13
REFERENCES . . . . .	58

PRECEDING PAGE BLANK-NOT FILMED

## FIGURES

No.		Page
1	Effects of Configuration Changes on Thrust Augmentation Ratio, $\phi$ . . . . .	15
2	Effects of Configuration Changes on Weight Flow Ratio . . . . .	16
3	Spark Shadowgraph of Baseline Configuration . . . . .	17
4	Schematic- Nozzle and Ejector . . . . .	18
5	Schematic -Test Apparatus . . . . .	19
6	Test Apparatus . . . . .	20
7	Nozzle Throat Length and Base Area Variations . . . . .	21
8	Primary Nozzle Turbulence Generator . . . . .	22
9	Location of Primary and Secondary Plenum Pressure Ports . . . . .	23
10	Ejector and Primary Nozzle Details . . . . .	24
11	Primary Exit Total Pressure Rake . . . . .	25
12	Total Pressure Survey of Primary Exits ( $P_{Tp}/P_{amb} = 4.0$ ) . . . . .	26
13	Total Pressure Profiles, Primary and Secondary Flows, Showing Flow Circulation . . . . .	27
14	Turbulence Intensities at Nozzle Centers-Baseline . . . . .	28
15	Primary Nozzle Turbulence Intensity Profiles . . . . .	29
16	Baseline Nozzle Performance Without Ejector . . . . .	30
17	Baseline Nozzle Performance With Ejector . . . . .	31
18	Baseline Nozzle With Ejector, Secondary Weight Flow, Thrust, and Weight Flow Augmentation . . . . .	32
19	Spark Shadowgraph Photos of Baseline Nozzle With Ejector . . . . .	33
20	Long Throat Nozzle Performance Without Ejector . . . . .	34
21	Long Throat Nozzle Performance With Ejector . . . . .	35
22	Long Throat Nozzle With Ejector, Secondary Weight Flow, Thrust, and Weight Flow Augmentation . . . . .	36
23	Spark Shadowgraph Photos of Long Throat Nozzle With Ejector . . . . .	37
24	Thick Base Nozzle Performance Without Ejector . . . . .	38
25	Thick Base Nozzle Performance With Ejector . . . . .	39
26	Thick Base Nozzle With Ejector, Secondary Weight Flow, Thrust, and Weight Flow Augmentation . . . . .	40
27	Spark Shadowgraph Photos of Thick Base Nozzle With Ejector . . . . .	41
28	High Turbulence Nozzle Performance Without Ejector . . . . .	42
29	High Turbulence Nozzle Performance With Ejector . . . . .	43
30	High Turbulence Nozzle With Ejector, Secondary Weight Flow, Thrust, and Weight Flow Augmentation . . . . .	44
31	Spark Shadowgraph Photos of High Turbulence Nozzle With Ejector . . . . .	45
32	Comparison of Experimentally and Analytically Determined Augmentation Ratios . . . . .	46
33	Typical Total Pressure Profiles . . . . .	47
34	Typical Static Pressure Profiles . . . . .	48
35	Profile Integrated Weight Flow Compared With Actual Values-Baseline Nozzle . . . . .	49



## FIGURES—Concluded

No.		Page
36	Profile Integrated Weight Flow Compared With Actual Values—Long Throat Nozzle . . . . .	50
37	Profile Integrated Weight Flow Compared With Actual Values—Thick Base Nozzle . . . . .	51
38	Profile Integrated Weight Flow Compared With Actual Values—High Turbulence Nozzle . . . . .	52
39	Axial Static Pressure Distribution on Ejector Sidewall—Baseline Nozzle . . . .	53
40	Axial Static Pressure Distribution on Ejector Sidewall—Long Throat Nozzle . .	54
41	Axial Static Pressure Distribution on Ejector Sidewall—Thick Base Nozzle . . .	55
42	Axial Static Pressure Distribution on Ejector Sidewall—High Turbulence Nozzle . . . . .	56
43	Composite Shadowgraphs of Correlation of Terminal Shock Location With Static Pressure Rise, $P_{TP}/P_{\infty} = 4.0$ . . . . .	57

## ABBREVIATIONS AND SYMBOLS

$A_b$	Primary nozzle base area
$A_c$	Ejector cross-sectional area
$A_p$	Primary nozzle area
$C_D$	Discharge coefficient: $\frac{w_p}{\text{Ideal primary weight flow}}$
$C_f$	Boundary layer skin friction coefficient
$C_{fg}$	Gross thrust coefficient: $\frac{\text{Measured thrust}}{(w_p/g)(\text{Ideal primary velocity})}$
$C_p$	Specific heat
$E$	Hot wire mean bridge voltage (with flow)
$E_o$	Hot wire mean bridge voltage (without flow)
$e'$	Root mean square (rms) value of bridge voltage fluctuations
$(L/D)$	Length-to-diameter ratio of equivalent cylindrical ejector with concentric primary. (Used to calculate internal skin friction drag in 1-D ejector analysis)
$M$	Mach number
$P_{amb}, P_\infty$	Ambient static pressure
$P_{TP}$	Primary total pressure
$P_{TS}$	Secondary total pressure
$P_{wall}$	Ejector wall static pressure
$U$	Mean axial velocity
$u'$	Root mean square (rms) value of axial velocity fluctuations
$W_{INT}$	Ejector weight flow (integrated from profile measurements)
$W_p$	Measured primary weight flow
$W_s$	Measured secondary weight flow
$\phi$	Ejector augmentation ratio: $\left[ \frac{C_{fg} \text{ with ejector}}{C_{fg} \text{ without ejector}} \right]_{P_{TP}/P_{amb} = \text{constant}}$

## 1.0 INTRODUCTION

That the turbulence level in the nozzle exit flow field can affect the spread of a jet has long been recognized. Measurements of turbulent jets have usually been made in the self-preserving region; i.e., that part of the jet sufficiently far downstream that the initial conditions have been washed out. Since typical ejectors consist of ducts surrounding the jet only for 10 or so nozzle diameters downstream and any self-preserving region begins far downstream of this, it is reasonable to expect that ejector mixing and performance are affected by the condition existing at the exit of the primary nozzle. However, in spite of the current and continuing interest in ejector systems, no work has been done to determine what effect, if any, results from the initial primary condition.

A number of prior investigators have observed or examined the effect of initial conditions on free jets. Cuadra and Ranner (ref. 1) noted that the jet from a nozzle with a rough internal surface spread more rapidly than one from a nozzle with identical but smooth contour. Bradshaw (ref. 2) investigated the effect of the state of the upstream nozzle boundary layer (whether laminar or turbulent) on the initial free mixing region in terms of the mean flow, turbulence, and noise generated. Chapman (ref. 3) and Wygnanski and Hawaleshka (ref. 4) performed analytical investigations on the effect of the initial mean velocity profile on the downstream development of the free shear layer. Most recently, Foss and Kleis (ref. 5) carried out an experimental investigation of the effect on free jet mixing of initial jet turbulence. To date, however, no work has been done concerning the effect on ejector jet mixing of upstream flow conditions. Oseberg and Kline (ref. 6), in an investigation of upstream conditions on free jet mixing, concluded that no benefits to ejector performance would result from variation of the initial jet conditions. This conclusion was based on a calculation of energy transmission from the low Reynolds number jet flow using their experimentally determined velocity profiles.

Ejector nozzles have been and continue to be considered for aircraft use as either noise suppressors or thrust augmentors. Typically, the investigation of ejector application for an airplane consists of a model-scale experimental development followed by a full-scale demonstration of the design. However, a number of factors change between model- and full-scale tests and are usually not accounted for. Notably, the turbulence intensity of the flow from a full-scale jet engine is usually higher than that from a model-test rig; the large-scale nozzle is fabricated of material which occupies a smaller fraction of the total ejector area than the model scale, and finally, the mean flow velocity profile between model and full scale may be different. The extrapolation of model-scale results to predict full-scale ejector performance is then subject to uncertainty because of the unknown effects of these initial conditions on the ejector performance. Thus, it was decided to carry out a test program in which these quantities are varied independently and to observe the resultant effects on the flow field and performance of the ejector.

## 2.0 TEST DESCRIPTION

It was decided to investigate the effects of initial flow conditions on the thrust and pumping performance of constant area ejectors typically considered for SST jet noise suppressors. The test was designed to permit direct measurement of the entrained secondary flow and system thrust as used in the measurement of velocity (i.e., pressure) profiles within the ejector. Additionally, it was desired to take spark shadowgraph photos of the ejector internal flow fields, and to permit this the ejector was made two dimensional.

In order to model the multiple primary elements encountered in jet noise suppressors, a five-element nozzle array was selected. This number of elements made available a center mixing region for measurement which was isolated from end wall effects by two other primary mixing regions. Additionally, this number of primary elements resulted in an ejector length which was practical from the standpoint of use on the Boeing high ratio test facility while maintaining high enough air flow rates to permit accurate performance determinations. A primary nozzle width of 0.5 in. was selected as a practical minimum if detailed flow surveys were to be made in its mixing region. The airflow limitations of the high ratio rig resulted in the width of a five-element array of these nozzles being 2.854 in. or a single nozzle aspect ratio of 5.708. This is a lower value than is typically used when measurements are made of two-dimensional jets and results in the ejector sidewall boundary layer affecting the internal flow profiles, as will be discussed in section 3.7.

### 2.1 RANGE OF VARIABLES

The test variables chosen were mean initial velocity profile, base thickness, and turbulence intensity in the primary stream. Two different conditions were run for each variable—one baseline condition and one variation from it, representing what was believed to be the maximum change in that variable to be encountered in actual practice. Only single variable changes were made; thus, a total of four configurations were run. These will be referred to as the baseline, long throat, thick base, and high turbulence configuration. It was intended that the long throat configuration vary the mean velocity profile by increasing the boundary layer thickness at the nozzle exit. The configurations are outlined in the following table:

Configuration	Throat length, in.	Base area/ primary area	Turbulence intensity
Baseline	0	0.037	0.02 primary 0.04 secondary
Long throat	6	0.035	0.025 primary 0.04 secondary
Thick base	0	0.25	0.02 primary 0.04 secondary
High turbulence	0	0.037	0.08 primary 0.04 secondary



The ejector area ratio,  $A_e/A_p$ , was 3.125, typical of those ejectors examined for use as noise suppressors for an SST application. The ejector length, equal to 30 primary nozzle heights, was also chosen as representative of a typical SST application employing a multitube suppressor.

The range of primary pressure ratios,  $P_{Tp}/P_{amb}$ , was from 1.5 to 4.0, while the secondary pressure ratio was held to unity to simulate the entrainment of flow from ambient pressure. Thrust and weight flow characteristics were measured over the above range in 0.5 increments in primary pressure ratio. Spark shadowgraphs were also taken at these conditions. Internal flow profiles were measured at primary pressure ratios of 1.5, 2.0, 3.0, and 4.0.

## 2.2 TEST HARDWARE

It was decided to investigate two-dimensional flows because of the ease of taking flow visualization photos through the plane sidewalls. A five-element primary nozzle configuration was chosen to more closely simulate the real case of a multielement suppressor, both in terms of merging adjacent mixing regions and the amount of ejector shroud area producing a drag on the mixed flow. Both primary and secondary flow paths were integrated into a single nozzle block. This block was made up of laminates containing two-dimensional primary and secondary flow paths that are exact reflections of one another about the center plane of the block. The nozzle block, ejector, and traversing probe are shown in the diagram in figure 4. Primary and secondary flows are separated by thin stainless steel plates. The purpose of this method of construction is to produce essentially parallel flows at the nozzle exit plane. An additional purpose of the laminated construction is to allow model versatility. Because there are three different thicknesses of lamination in the model, ejectors with three different area ratios may be constructed by a simple restacking of the laminates, still resulting in a five-element primary in the same ejector height. Ejector area ratios of 2.6, 3.2, and 4.3 are possible, though present testing is limited to the 3.2 ratio.

The flows into the primary and secondary sides of the nozzle block are from plenum chambers supplied by the primary and secondary flows of the high ratio rig. The flow paths are shown in the diagram in figure 5. Instead of dumping flow directly into the plenum, it is bled into the plenum more gradually from a set of holes in the supply pipe directed outwardly. The flow then reverses direction and enters the primary or secondary inlet slots in the nozzle block. The entire test apparatus is pictured in figure 6. The model is suspended from the ceiling because of weight limitations on the high ratio rig.

The methods by which the base area and initial velocity profile are varied are diagrammed in figure 7. Two separate sets of divider plates allow changes in the initial base area separating the two flows. An additional laminate was fabricated that allowed the nozzle throat to be extended 6 in. to produce a different initial mean velocity profile.

Initial turbulence intensity was increased by installing the blockages shown in figure 8 upstream of the nozzle exit. Hot wire measurements were made to verify the resulting values of turbulence intensity.



## 2.3 INSTRUMENTATION

In this test, bulk flow quantities (primary and secondary flow and system thrust) as well as detailed flow fields were measured. In addition, the axial static pressure distribution on the ejector wall was measured. Primary and secondary weight flows were measured with ASME flow nozzles of 3.000-in. and 2.751-in. dia, respectively. The system thrust was measured with a strain gage type load cell. Primary and secondary total pressures were sensed at one of the five pressure taps installed in each plenum chamber (fig. 9). Ejector wall static pressure taps were located in one of the plexiglas ejector sides (fig. 10).

A total pressure probe was traversed across the central jet of the primary nozzle array to obtain velocity profiles. This probe consisted of a 0.5-in. length of 0.026 o.d. hypodermic tubing protruding beyond some 0.040 o.d. tubing into which it was brazed. The larger tube itself was brazed into 0.0625 o.d. tubing which ran the length of the support strut and connected to the instrumentation lines. Static pressure profile measurements were made by substituting a length of 0.040-in. tubing for the 0.026-in. total probe. This tubing was capped at one end with a streamlined fairing and contained four small holes drilled into the probe sides. Profile data were taken on an X-Y plotter and subsequently digitized for computer data reduction.

Spark shadowgraphs were made with collimated light produced by a 6-in. parabolic mirror with the spark located at the focus. An aerial camera magazine and a film plane were placed on the other side of the ejector from the light source, and both the spark source and film advance operated remotely during the test.

The flow turbulence was measured by means of a DISA 55D01 constant temperature hot wire anemometer unit using a subminiature probe with a tungsten element. The rms fluctuating voltage was read from a DISA rms voltage meter. The turbulence intensity,  $u'/U$  was calculated by the following relationship:

$$\frac{u'}{U} = \frac{4Ee'}{E^2 - E_0^2}$$

## 2.4 TEST PROCEDURE

The design of the test apparatus made it impossible to directly measure the total pressure of either stream. Instead, a number of static taps were built into each plenum chamber, and the average reading of these pressure taps was compared with the actual nozzle total pressure measured by a rake traversed across the nozzle exit. (This rake is shown in fig. 11.) The actual nozzle total pressure consisted of the average of the rake readings over the entire five-nozzle array, with the readings being taken at the center plane of each nozzle. The true average total pressure divided by the average of the plenum readings produced a ratio which was used in all subsequent testing to determine the nozzle total pressure from the plenum readings.

A single plenum pressure tap was chosen as most representative of the true nozzle total pressure, and this was subsequently used to set nozzle pressure ratio during the test.

The variation of each of the three test quantities required changes to the nozzle block itself; accordingly, for each variation of initial condition a baseline test run was made to obtain the nozzle performance without ejector. This performance was used in the calculation of ejector augmentation ratio.

Ejector nozzle performance, wall static pressure measurements, and spark shadowgraphs were made with the traversing probe assembly removed. With the probe installed, total and static pressure profiles were recorded. Additionally, performance data were also recorded at selected times during the taking of pressure profiles.

### 3.0 TEST RESULTS

#### 3.1 BASELINE CALIBRATION

Typical total pressure profiles at the midplanes of each of the primary nozzles are shown in figure 12. For approximately 80% of the nozzle width, little variation in total pressure occurs; for the remaining 20%, drops of around 7% can be seen in each nozzle. Traverses across the nozzle width show that this low pressure region occurs only in the midplane region.

A continuous traverse was made of the nozzles, recording the pressures at either end on an X-Y plotter. These plots are shown in figure 13. A dip in the total pressure at the nozzle center plane can be seen in each traverse nearest the center of flow curvature. This is caused by streamwise vorticity set up within the nozzles as the flow turns 90° from the nozzle inlet to the exit. This effect may be seen in both the primary and secondary flow passages.

The turbulence intensity in the middle of each primary and secondary passage is shown in figure 14. Because of the strength limitation of the hot wire itself, these measurements were made at a nozzle velocity of 300 fps. The higher level of turbulence intensity in the secondary stream can be explained by noting that the overall area contraction between the plenum chamber and the nozzle exit plane is less for the secondary than the primary flow. Thus, assuming that the same turbulence intensity initially exists in either plenum, when turbulent fluctuations are carried to the nozzle exit, they are a smaller fraction of the primary exit velocity than of the secondary because of the greater contraction in primary flow area. A profile of turbulence intensity is shown for the center nozzle in its midplane in figure 15. Here again, the effect of the streamwise vorticity caused by flow turning is evident. In this case, the higher values of turbulence intensity occur in the part of the nozzle exit where the low values of total pressure exist.

#### 3.2 BASELINE PERFORMANCE

The velocity and discharge coefficients of the baseline nozzle configuration without ejector are shown in figure 16. The velocity coefficients have been corrected for nozzle base pressure by adding a term calculated as  $(P_{amb} - P_b) A_s$  to the measured system thrust, where  $P_b$  is determined from the secondary plenum internal pressure. This corrects for the less than ambient base pressures in the secondary nozzles but cannot allow for a possible decreased base pressure on the remainder of the nozzle block. The increasing values of discharge coefficient with increasing pressure ratio are to be expected because of the deformation of the nozzle sidewall under pressure.

The velocity and discharge coefficients of the nozzle with ejector are shown in figure 17. In this and all succeeding cases with ejector, the secondary flow has been regulated to provide a pressure ratio,  $P_{TS}/P_{amb}$ , of 1.0. The shape of the velocity coefficient curve is similar to results from other ejectors in that it peaks at a low pressure ratio and decreases thereafter with increases in pressure ratio. The different shape of the discharge coefficient curve from the primary alone case is due to the lower pressure at the primary nozzle exits which exists when the ejector is installed. At below critical pressure ratio, the effect is to draw more

primary flow through the nozzle than would have occurred without the ejector. In addition, there is a greater pressure difference across the wall separating primary from secondary flow in the case of the ejector. This can be expected to produce larger wall deflections and a higher discharge coefficient with the ejector installed than without.

The entrained weight flow,  $W_S$ , is shown in figure 18 as a function of pressure ratio. The peak in this curve occurs at a pressure ratio somewhat lower than that at which the secondary flows, restricted by the primary jets at their maximum cross section, become sonic. The thrust augmentation and weight flow ratio are also shown in the same figure. The augmentation ratio is calculated as the ratio of velocity coefficients with and without ejectors at the same pressure ratio. The weight flow ratio, on the other hand, is calculated as the ratio between the secondary and primary flow rates with the ejector installed. Spark shadowgraphs of the flows in the baseline ejector are shown in figure 19. An area, including the nozzle exit, illuminated by the 6-in.-dia collimated flash is shown. The flow direction is from left to right, and the upper three primary jets are visible. Normal shocks first appear in the jet near  $P_{Tp}/P_{amb} = 2.0$  and then become more numerous and pronounced as pressure ratio is increased. At a certain pressure ratio, in this case  $P_{Tp}/P_{amb} = 3.0$ , the secondary has become sonic at the station of its minimum area. Downstream of this, a normal shock occurs, and this pressure change is transmitted into the primary flow as an oblique shock which then terminates in a normal shock. After the first normal shock, the secondary flow apparently remains subsonic. At still higher pressure ratios, the shocks in the secondary streams produce weak oblique shocks in the primary streams. These shocks repeat themselves farther downstream in the same manner as the more familiar repeated system of normal shocks in an undeveloped free jet. This shock structure carries through the downstream secondary flow as repeated normal shocks. The network of weak oblique shocks in the primary gives way to what appears to be a normal shock farther downstream, after which the flow appears largely chaotic. This normal shock is related to the beginning of the pressure rise to ambient required of an ejector operating with subsonic flow at its exit. This will be further discussed in section 3.7, describing mixing profiles and static pressure distribution.

### 3.3 LONG THROAT CONFIGURATION

The velocity and discharge coefficients of the long throat nozzle array without ejector are shown in figure 20. Both quantities are, as expected, lower than the corresponding baseline nozzle values because of the friction of the additional throat length. The same two quantities for the nozzle with ejector are shown in figure 21. The thrust augmentation ratio, the secondary weight flow, and the weight flow ratio are shown in figure 22, compared to the superimposed values of the baseline nozzle. The thrust augmentation ratio of the long throat nozzle is substantially lower than that of the baseline. This is explained in part by the 6 in. additional duct length of the long throat nozzle creating pressure loss in the secondary flow. Any difference between the baseline and long throat nozzle configuration is, therefore, a result of the effect of the initial mean velocity profile. The entrained flow rate of the long throat configuration can be seen to peak at higher pressure ratios than the baseline nozzle. In both cases the flow limitation producing this peak results from the restriction of the secondary flow area by the expansion of the primary flow. In the case of the long throat nozzle, primary flow would, for a given pressure ratio, expand to fill a smaller area, i.e., provide less restriction to the secondary, and hence the secondary flow rate would peak at a higher pressure ratio. For the same reason, the weight flow ratio of the long throat nozzle is greater than that for the

baseline at the higher pressure ratios. Spark shadowgraphs of the ejector flow fields with the long throat nozzle are shown in figure 23 for a series of pressure ratios. The same general features of the flow can be seen in these photos as in those of the baseline nozzle. However, in the case of the long throat configuration it should be noted that the first appearance of shock in the secondary flow occurs at a primary pressure ratio of 3.5 compared to 3.0 for the baseline. This is again indicative of the lower overall total pressure of the primary of the long throat configuration for a given setting in primary total pressure ratio.

### 3.4 THICK BASE CONFIGURATION PERFORMANCE

The thrust and discharge coefficients of the thick base nozzle configuration are shown in figure 24. While the discharge coefficient of the nozzle is the same as the baseline, the thrust coefficient is about 0.75% higher. No reason for this can be given. If, however, this number is treated at the uncertainty band which must be applied to all results, the test conclusion will not be altered. The thrust and discharge coefficients of the thick base nozzle with ejector are given in figure 25. The thrust coefficient is lower than the baseline ejector nozzle and the discharge coefficient is, again, the same value. The thrust augmentation ratio, secondary weight flow, and weight flow ratio of the ejector are given in figure 26 with the corresponding values for the baseline nozzle superimposed. The thrust augmentation ratio is lower than the baseline value because of the increased drag producing area of the splitters. Both the secondary weight flow and secondary-to-primary weight flow ratio are lower at the lower pressure ratio than at the baseline. At the inlet of the ejector nozzle the extra base thickness represents a restriction of the secondary flow at lower primary pressure ratios. Then at higher pressure ratios the restriction becomes instead the expansion of the primary jet which is relatively unaffected by the base thickness and instead dependent on nozzle area ratio and primary pressure ratio. Spark shadowgraph photos of the ejector flow field are shown in figure 27 for a series of primary pressure ratios. During the run, a sealant compound was drawn into the ejector, causing the dark shadows in the secondary. The most apparent difference between the thick base configuration and the baseline is the generation of additional shock waves in the primary flow at the end of the base recirculation region. At higher pressure ratios these shocks lead to an earlier termination of the supersonic ejector flow regime and recompression to subsonic flow than the baseline. This will be discussed in section 3.7.

### 3.5 HIGH PRIMARY TURBULENCE—PERFORMANCE

The effects of high initial primary turbulence levels were investigated by the introduction of turbulence into the primary flow by means of upstream obstruction. At first, an upstream choke plate located at the inlet side of the primary nozzle block was used. This plate was modified by trial and error until a uniform total pressure profile was obtained across the nozzle. At that point, the turbulence level was measured across the width of the nozzle and found to be highly nonuniform varying from  $u'/U = 0.13$  at the outside of the turn to 0.04 at the inside. The performance of this configuration with ejector was nevertheless measured. Then, an attempt was made to build a more even profile of turbulence intensity by inserting sets of rods in the primary flow passage. This increased the value of turbulence intensity at the low end somewhat, and again performance was measured. In each case, the calibration described in section 2.4 was redone to ensure that the high turbulence model was tested at the same primary total pressure as the baseline. No difference was noted between the two high turbulence models.



The thrust and discharge coefficients of the high turbulence configuration ( $u'/U = 0.08$  averaged over the nozzle width) are shown in figure 28. These quantities are the same as those of the baseline nozzle. Thrust and discharge coefficients of the nozzle with ejector are shown in figure 29. The discharge coefficient of the high turbulence model is substantially the same as the baseline. The thrust coefficient is greater throughout the range of pressure ratios tested. Augmentation ratio, secondary weight flow, and weight flow ratio are shown in figure 30. Each of these quantities is somewhat higher for the case of high initial turbulence than the baseline case. These changes can be explained only as an enhancement of the mixing rate by the higher initial turbulence. In view of the rather extreme measures taken in this test to increase flow turbulence, the results indicate that it will not generally be a factor in model-scale testing because of the usual efforts made to ensure smooth flow. Its effect on the extrapolation of model- to full-scale results requires determination of the actual turbulence level at the exit of full-scale jet engines. Spark shadowgraphs of the ejector with high turbulence primaries are shown in figure 31. The flow patterns are similar to the baseline nozzle except that the supersonic flow region in the ejector persists further downstream in the case of high primary turbulence.

### 3.6 COMPARISON WITH 1-D EJECTOR THEORY

While the original purpose of the test was to investigate the effect of initial conditions on the mixing process of an ejector nozzle, it became apparent that some of the effects noted could be explained by a simple 1-D analysis of the ejector without resorting to a study of the mixing process itself. This can be seen from figure 32 which shows the thrust augmentation for the baseline, long throat, and thick base configurations, together with analytically predicted performance values. The marked point at  $P_{Tp}/P_{amb} = 2.0$  on the augmentation ratio of the baseline nozzle is a point of forced agreement. At this point, the secondary total pressure loss used in the analysis was varied until agreement was forced between analysis and experiment. All subsequent data were calculated with this value of secondary flow total pressure loss, except for the long throat nozzle for which the additional loss due to the 6-in. throat extension was calculated analytically. The following table lists the geometric and flow parameters used in the analysis for the calculation of the curve shown.

	Baseline	Long throat	Thick base
Freestream Mach no.	0	0	0
Primary Mach no.	1	1	1
$P_{T}/(secondary)$	0.185	0.297	0.185
$A_e/A_p$	3.24	2.24	3.24
(L/D) effective	3.54	3.54	3.54
$C_f$	0.004	0.004	0.004
$A_b/A_p$	0.039	0.039	0.246

The augmentation ratio is adequately predicted for the baseline nozzle, as would be expected, because of the procedure of forcing agreement at one point on the curve. The thick base augmentation ratio is also predicted well; however, agreement is not as good for the long

throat nozzle, but it can be seen that the extra loss in the secondary flow because of the increased nozzle thrust length accounts for a substantial part of the difference between the performance of the long throat configuration and that of the baseline.

### 3.7 MIXING PROFILES AND STATIC PRESSURE DISTRIBUTIONS

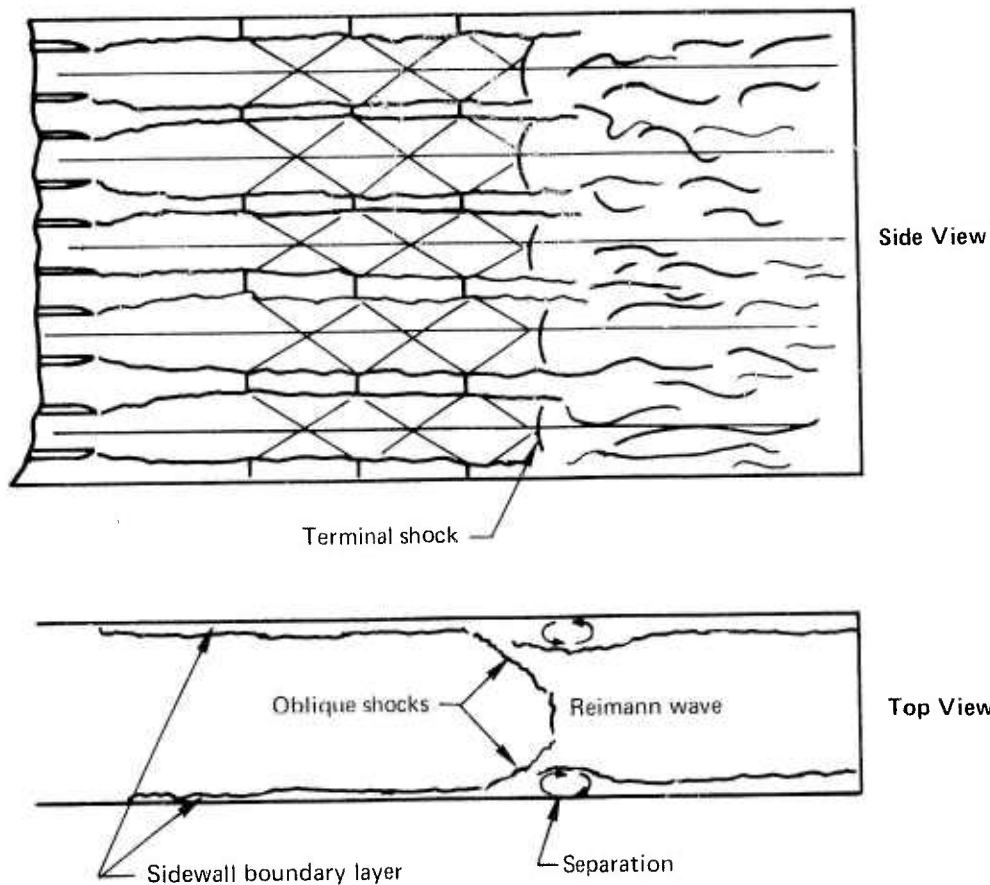
Total and static pressure profiles were taken of the center jet from the center of one adjacent secondary passage across the jet to the center of another. Typical total and static pressure profiles are shown in figures 33 and 34. These were digitized and converted to punched cards for computer data reduction. Where required, the indicated total pressure was corrected for the normal shock ahead of the total pressure tube.

From the true total pressure and Mach number as well as the flow total temperature, integrated weight flows were obtained, assuming symmetry and two dimensionality of the flow. This was done to provide a check of the accuracy of the profile measurements. The integrated value of weight flow divided by the sum of primary and secondary weight flows measured by the ASME nozzles is shown for all configuration variations in figures 35 through 38. The integrated weight flow differs from the measured values by more than 20% at some stations. This, it is felt, casts a great deal of uncertainty on the value of the profile measurements for observing the effects of upstream initial conditions.

In almost all cases, the integrated weight flow is greater than the value actually measured. It is believed that the deviation of the integrated weight flow from that actually measured results from the assumption of two dimensionality employed in the integration. That is, the flows are actually three dimensional because of the growth of the ejector sidewall boundary layers. The boundary layer growth restricts the flow area available in the same manner as developing channel flow, and the velocities measured in the center are higher than the average. Thus, the sidewall boundary layer growth should produce a higher integrated weight flow than actual.

The axial static pressure distributions on the ejector sidewall are shown in figures 39 through 42. At the lower pressure ratios, the trend is as expected with a smooth, continuous increase in static pressure from the primary nozzle exit to the ejector exit. At higher pressure ratios, above that at which the secondary flow becomes choked, a different type of distribution is apparent wherein the static pressure remains relatively constant and at a low level for some distance downstream. It then rises very steeply to ambient pressure at the exit. The axial location of this pressure rise is definitely affected by the initial condition of the primary flow. A high initial turbulence level permits the low ejector pressures to be maintained farther downstream than any other configuration. On the other hand, both the thick base and long throat version maintain this low pressure for only a short distance downstream.

It is believed that a shock on the ejector sidewalls, not just the mixing process, produces the sudden pressure rise observed. This is borne out by an examination of figure 43 in which composite shadowgraphs are shown of each ejector operating at a pressure ratio of 4.0. Marked on each shadowgraph is the location at which the sudden pressure rise occurs. In each case this rise is about 2 in. upstream of the terminal shock in the primary jets. A shock on the ejector sidewall would have the form shown in the following diagram and then the normal shock in the primary flow might be a Reimann wave near two intersecting obliques. The pressure rise in the wall, while sudden, is still smoothed out by the wall boundary layer to prevent detection by the shadowgraph.



This final shock is a necessary recompression dividing the upstream supersonic ejector flow from the downstream subsonic one. If the back pressure of the ejector were lower, this recompression would occur either at the ejector exit or not at all, and the ejector would be operating completely supersonically.

## 4.0 CONCLUSIONS

These experiments have shown that the initial jet conditions can change the flow mixing process and overall performance. It is concluded that:

1. All three of the variables tested produced noticeable changes in thrust augmentation and pumping performance. If any of these initial conditions are different in the model-scale from full-scale nozzle system, the differences must be accounted for in the prediction of full-scale performance.
2. The effects of base thickness and throat length on performance are predictable with the proper one-dimensional flow analysis without consideration of the details of the mixing process. The effect of throat length on nozzle performance results from an additional loss in the secondary flow due to the long throat and the altered primary velocity profile. These effects were not clearly separated in this test.
3. Higher values of initial turbulence level in the primary produced large changes in the flow field as seen from shadowgraph and static pressure profiles. Slight increases in pumping and thrust performance also were seen. These effects are only explainable through detailed consideration of the mixing process and/or the ejector sidewall boundary layer.
4. The spark shadowgraph photos of the baseline configuration in figure 19 indicate that for pressure ratios greater than 3.5 a nearly uniform primary flow exists with a shock structure composed of weak oblique shocks. This suggests that the flow region may be adequately modeled by analyses that neglect transverse pressure gradients.

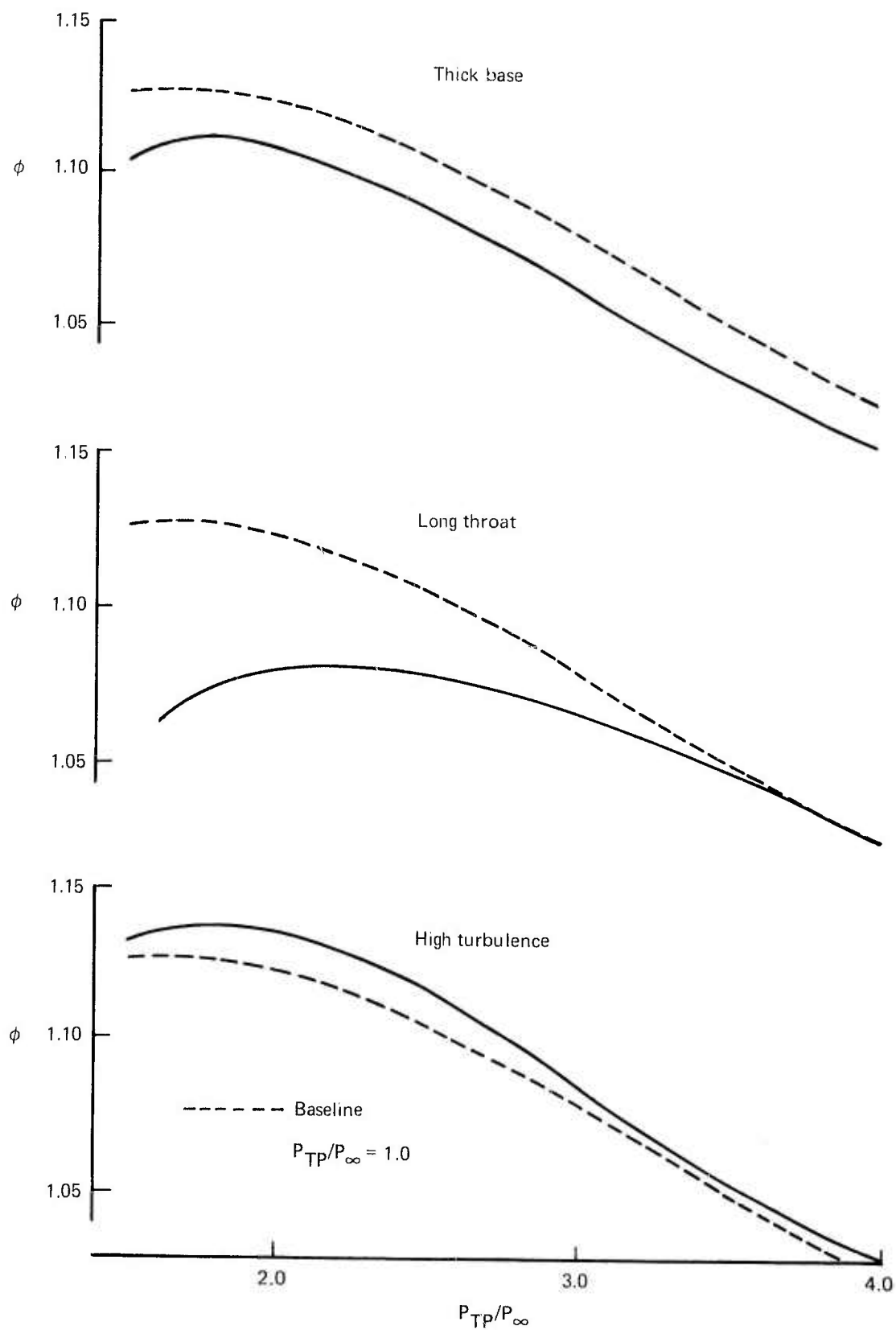


Figure 1.—Effects of Configuration Changes on Thrust Augmentation Ratio,  $\phi$



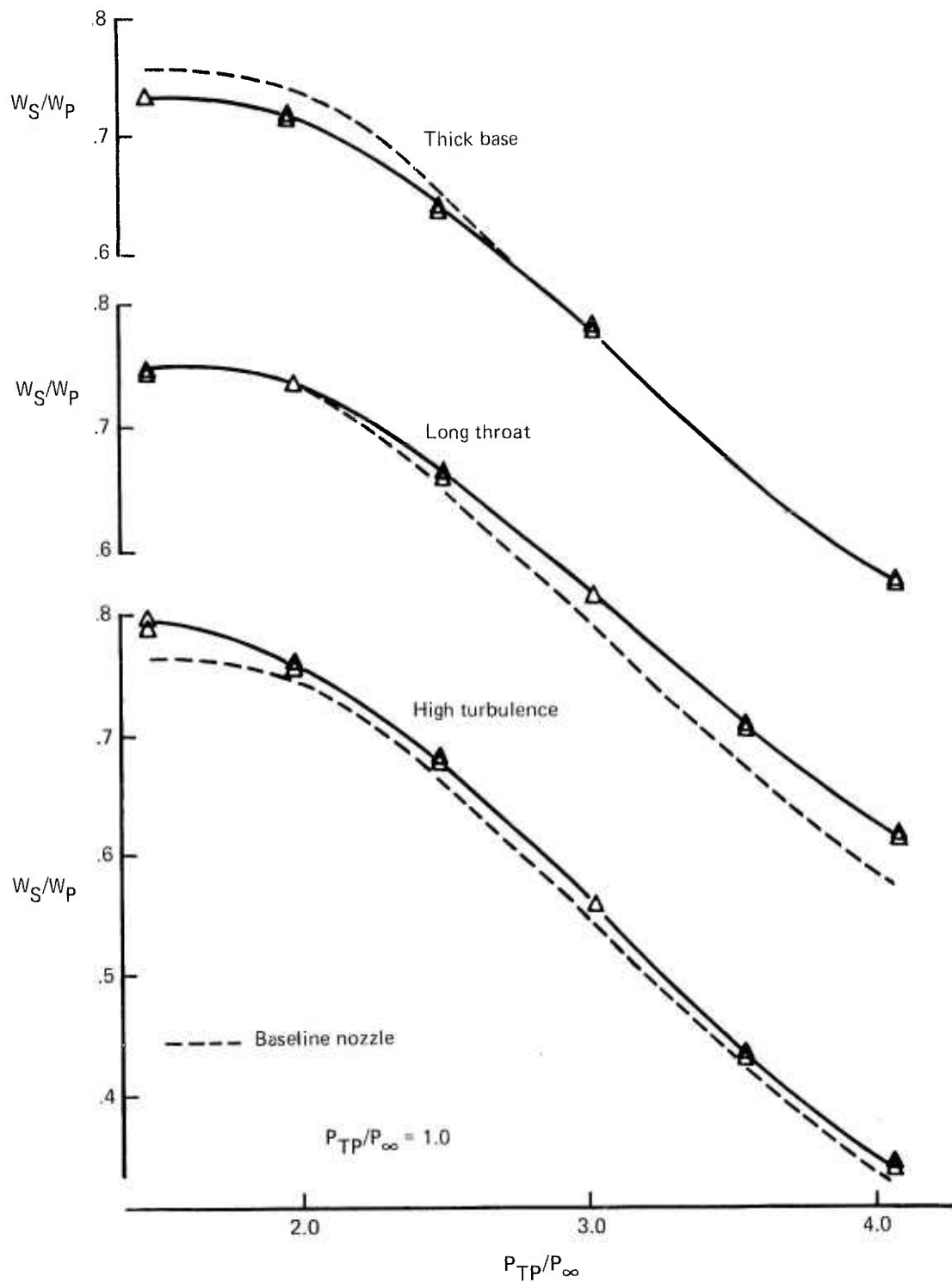


Figure 2.—Effects of Configuration Changes on Weight Flow Ratio

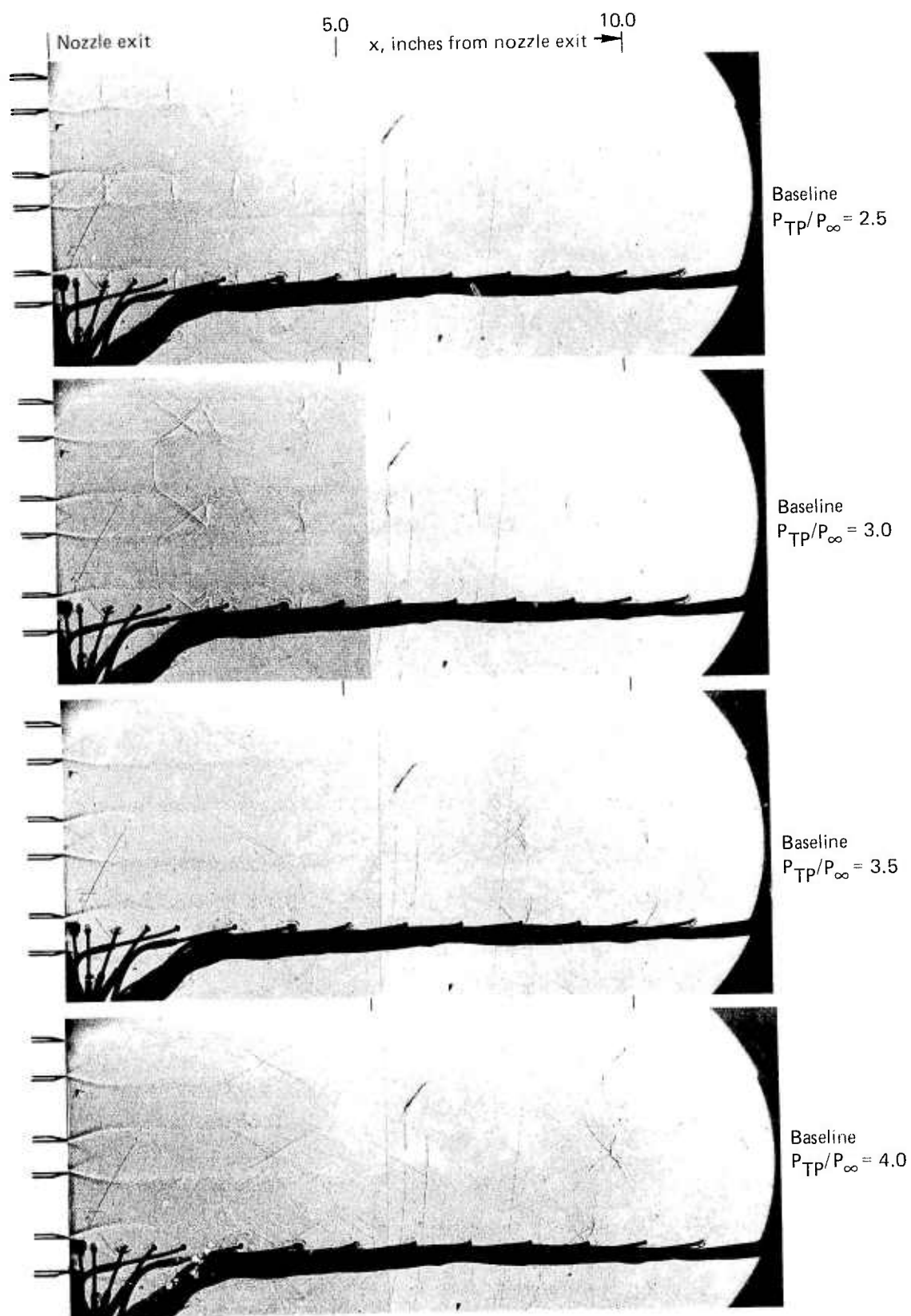


Figure 3.—Spark Shadowgraph of Baseline Configuration

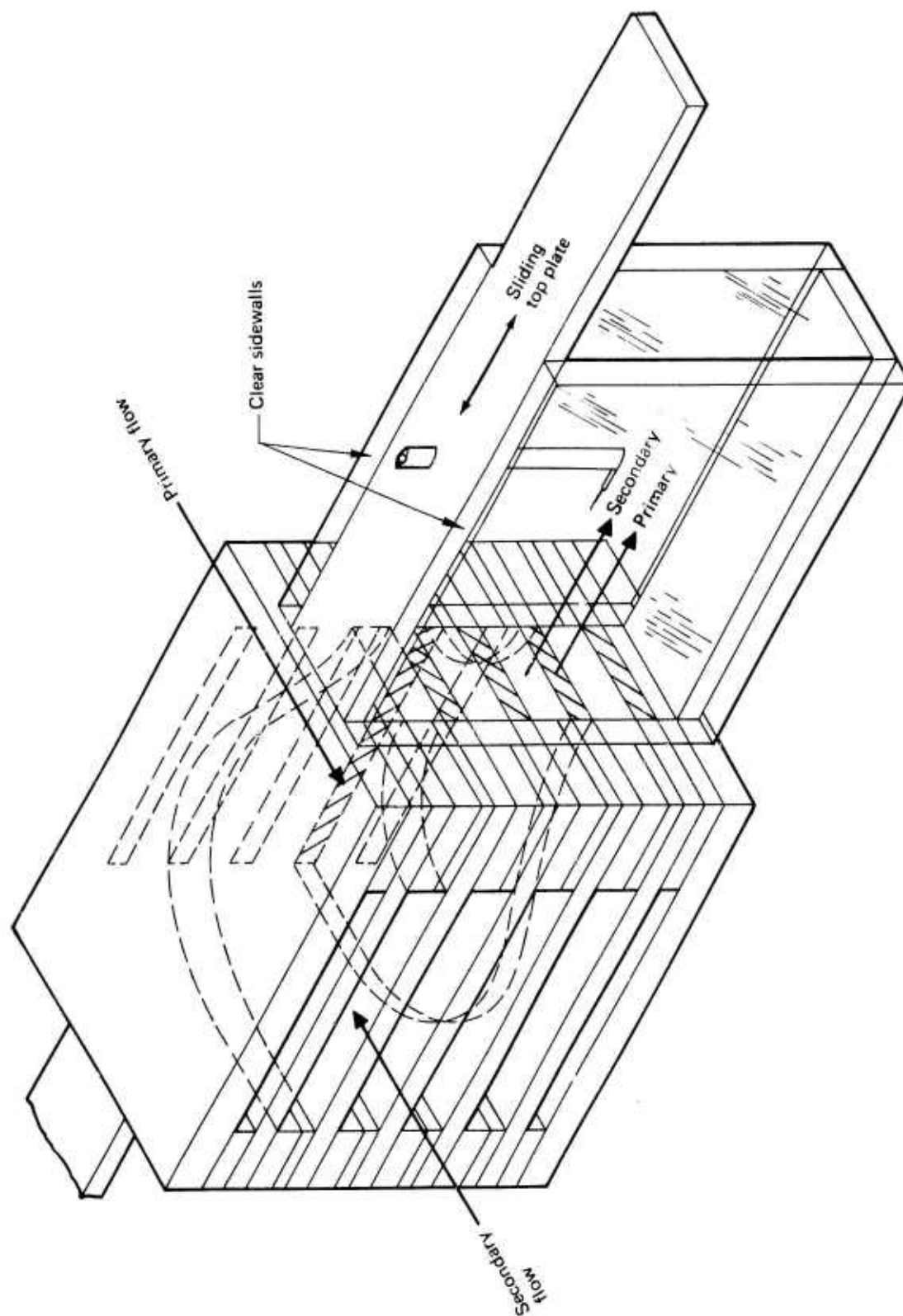


Figure 4.—Schematic—Nozzle and Ejector

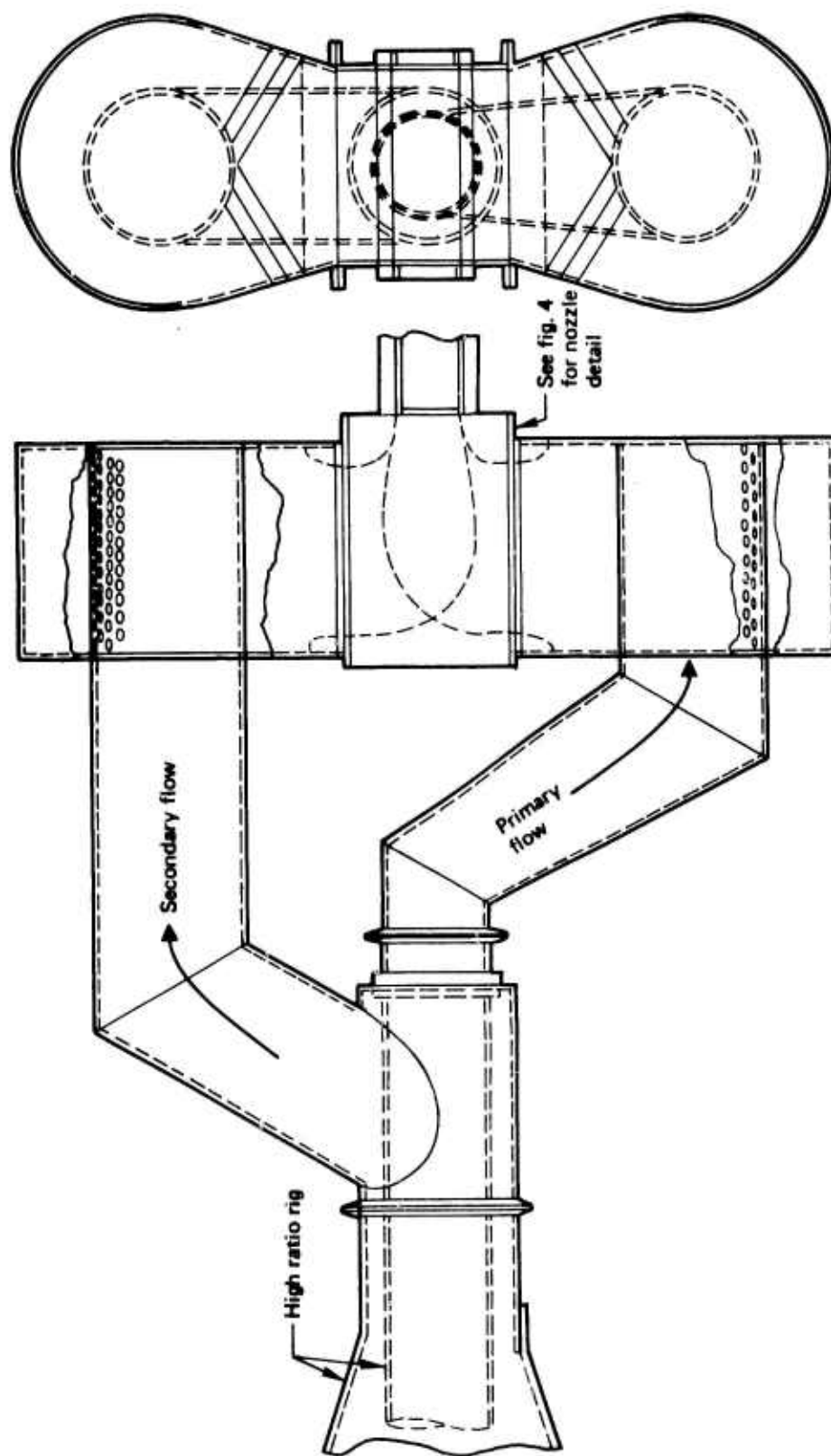


Figure 5.—Schematic—Test Apparatus

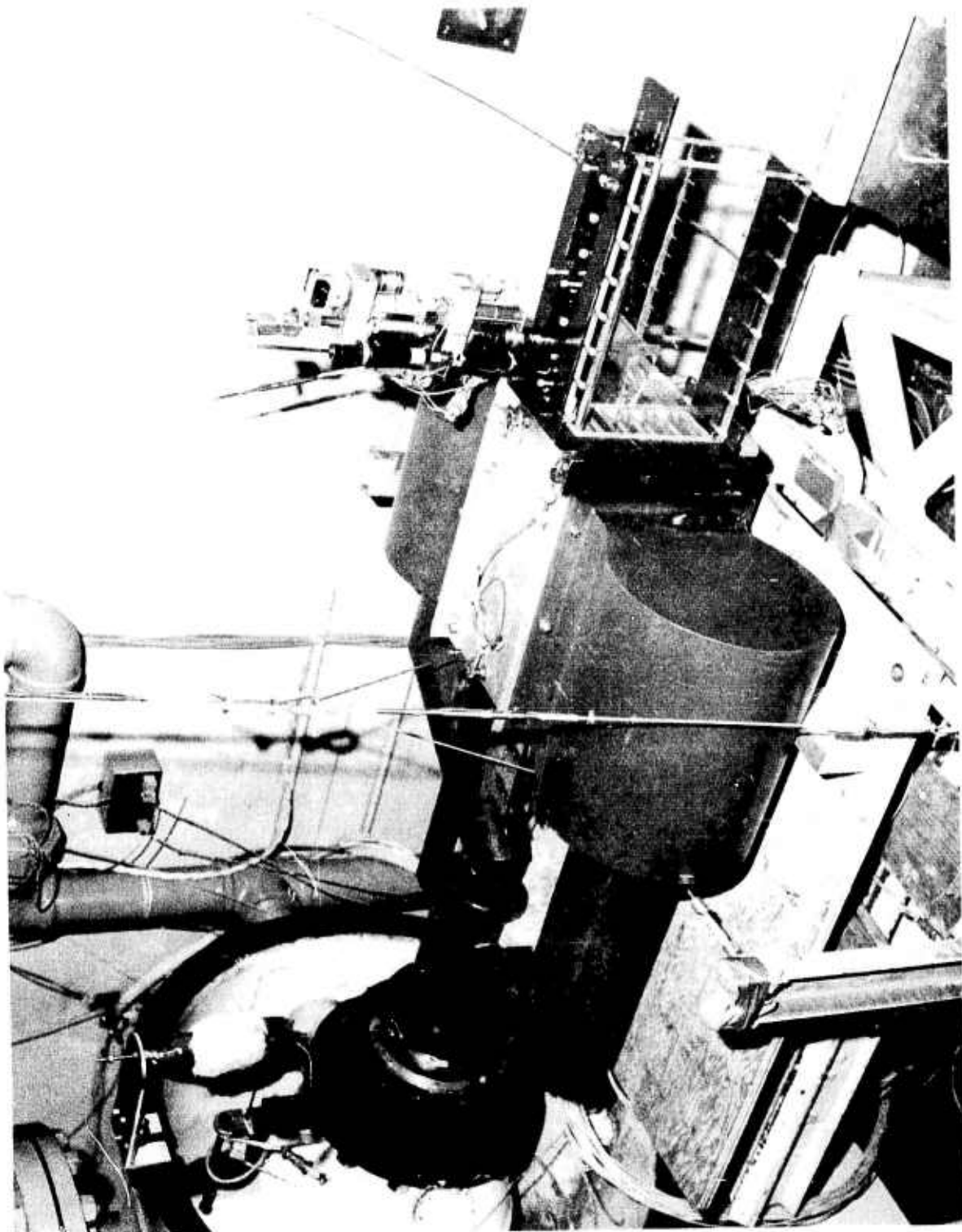


Figure 6. — Test Apparatus



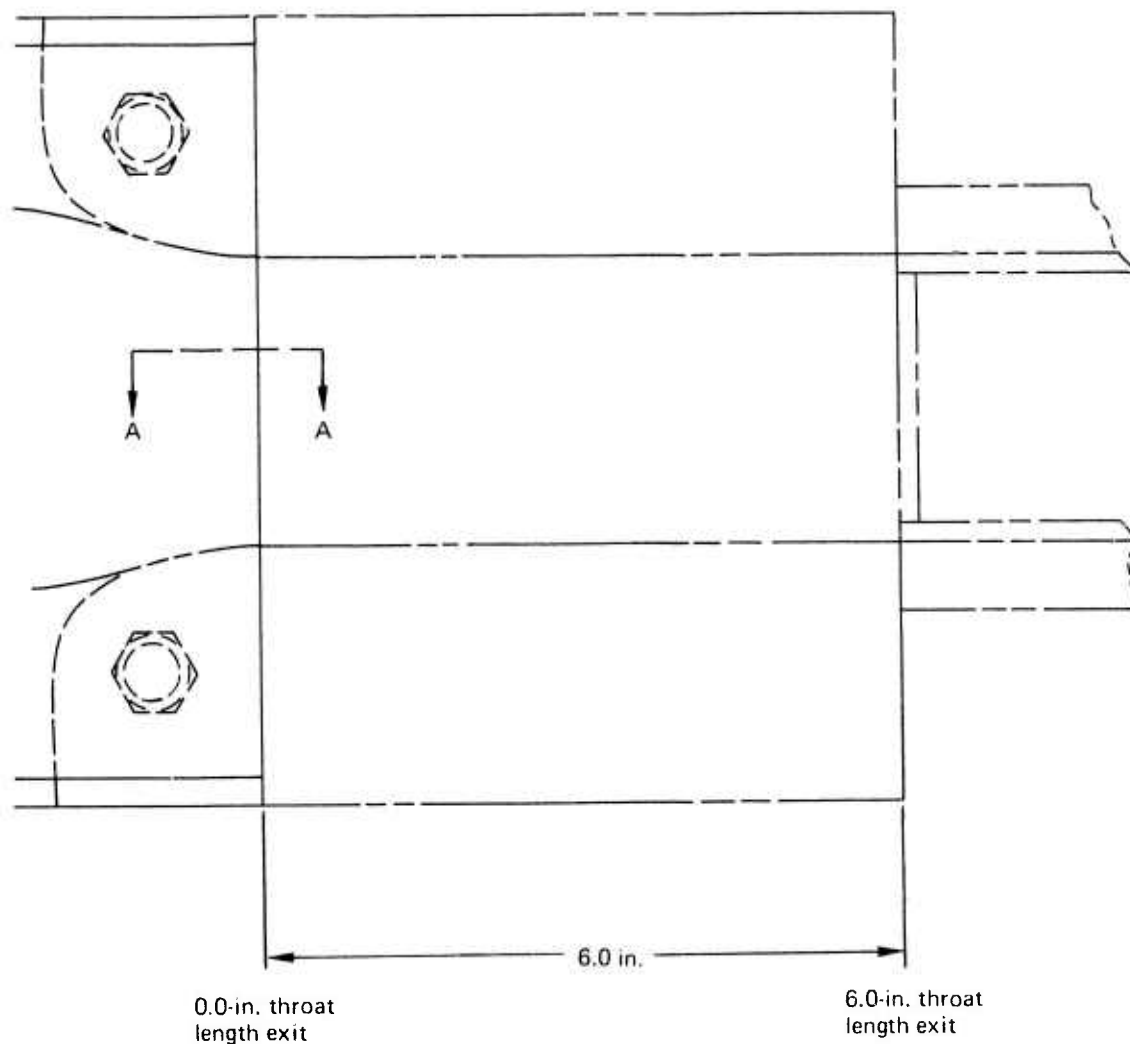
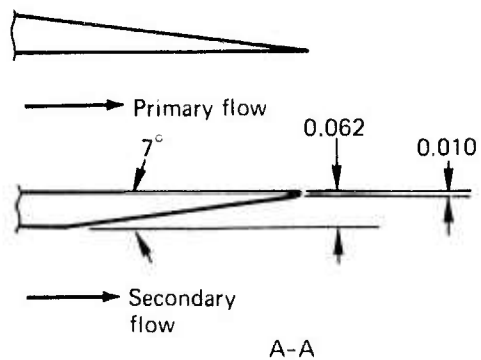


Figure 7.—Nozzle Throat Length and Base Area Variations

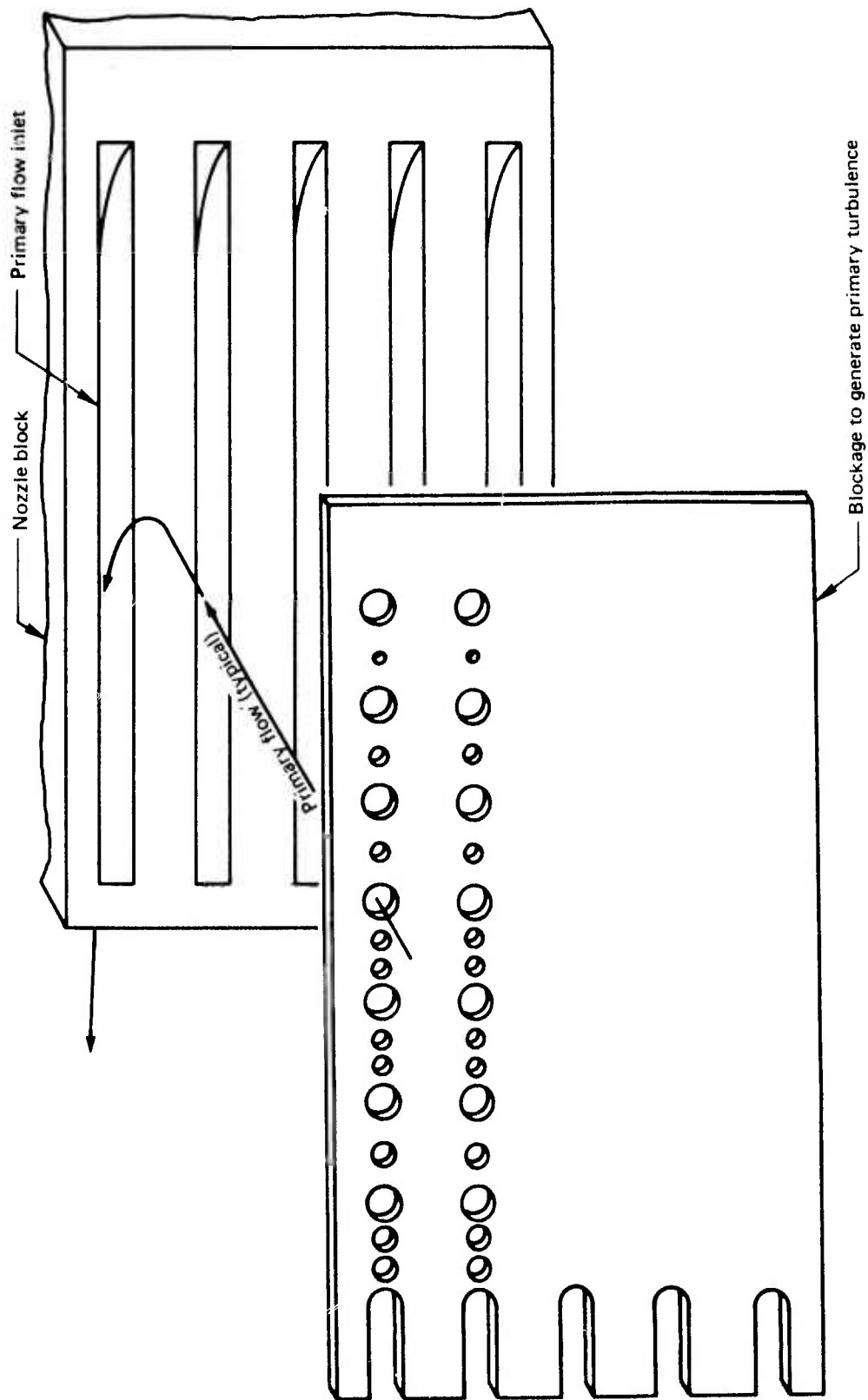


Figure 8.—Primary Nozzle Turbulence Generator

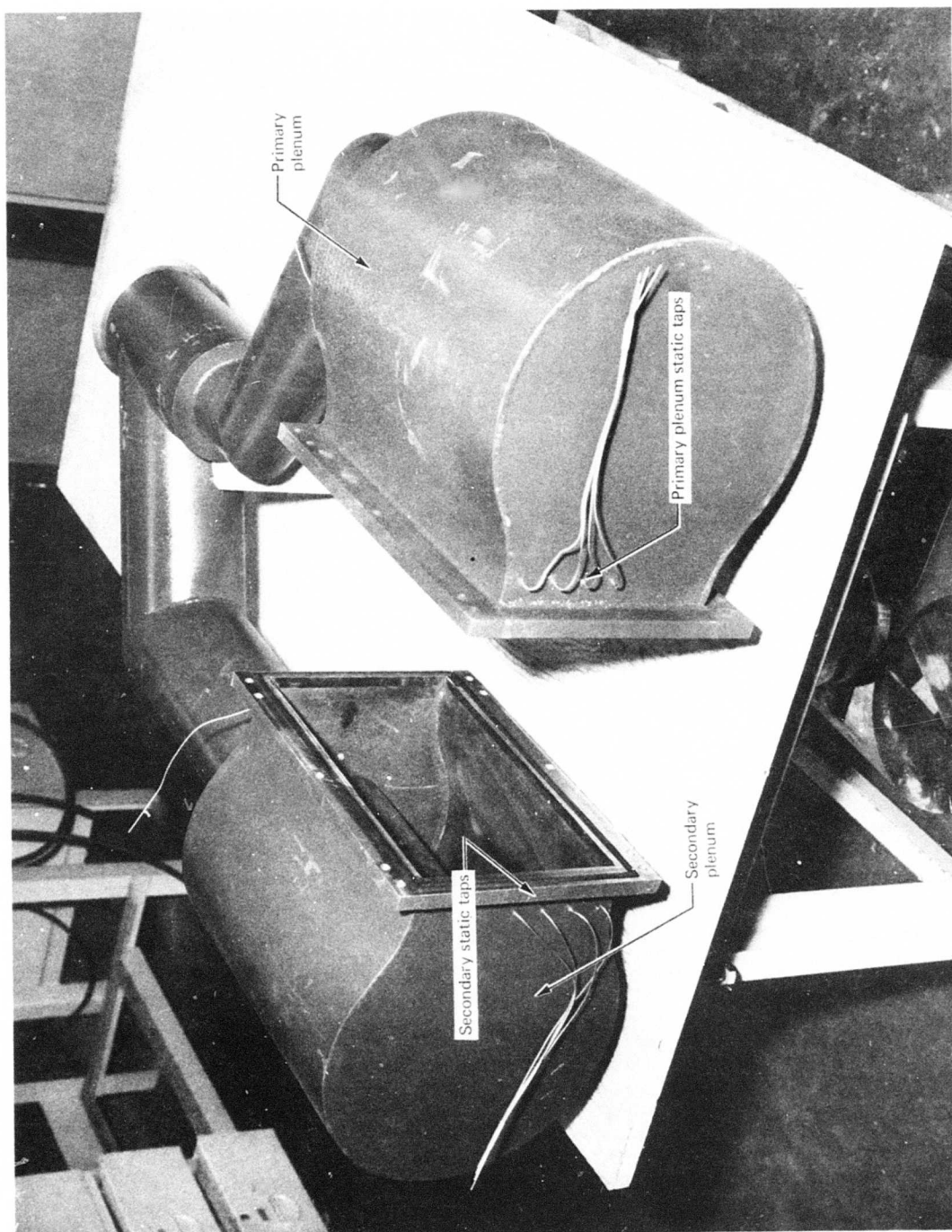
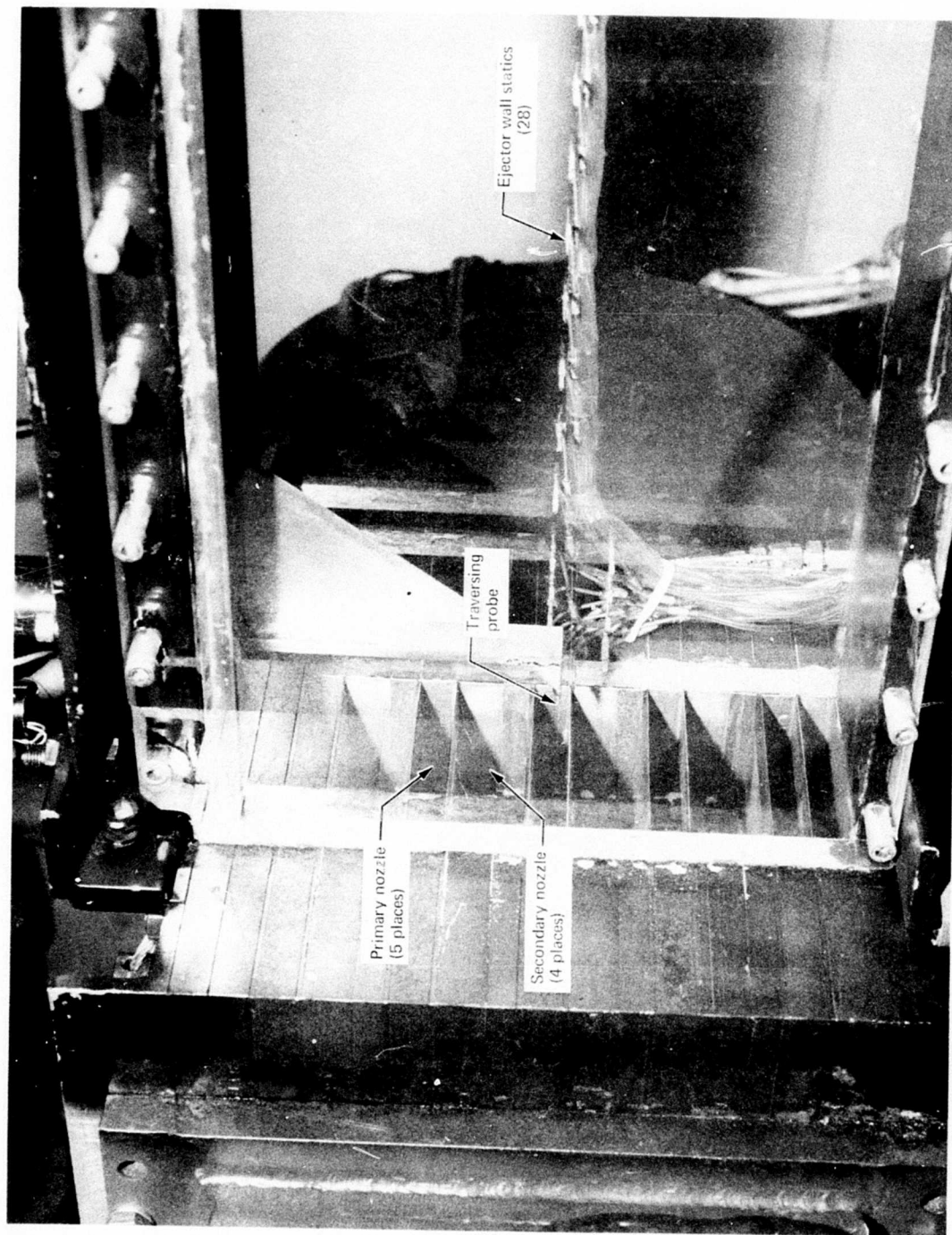
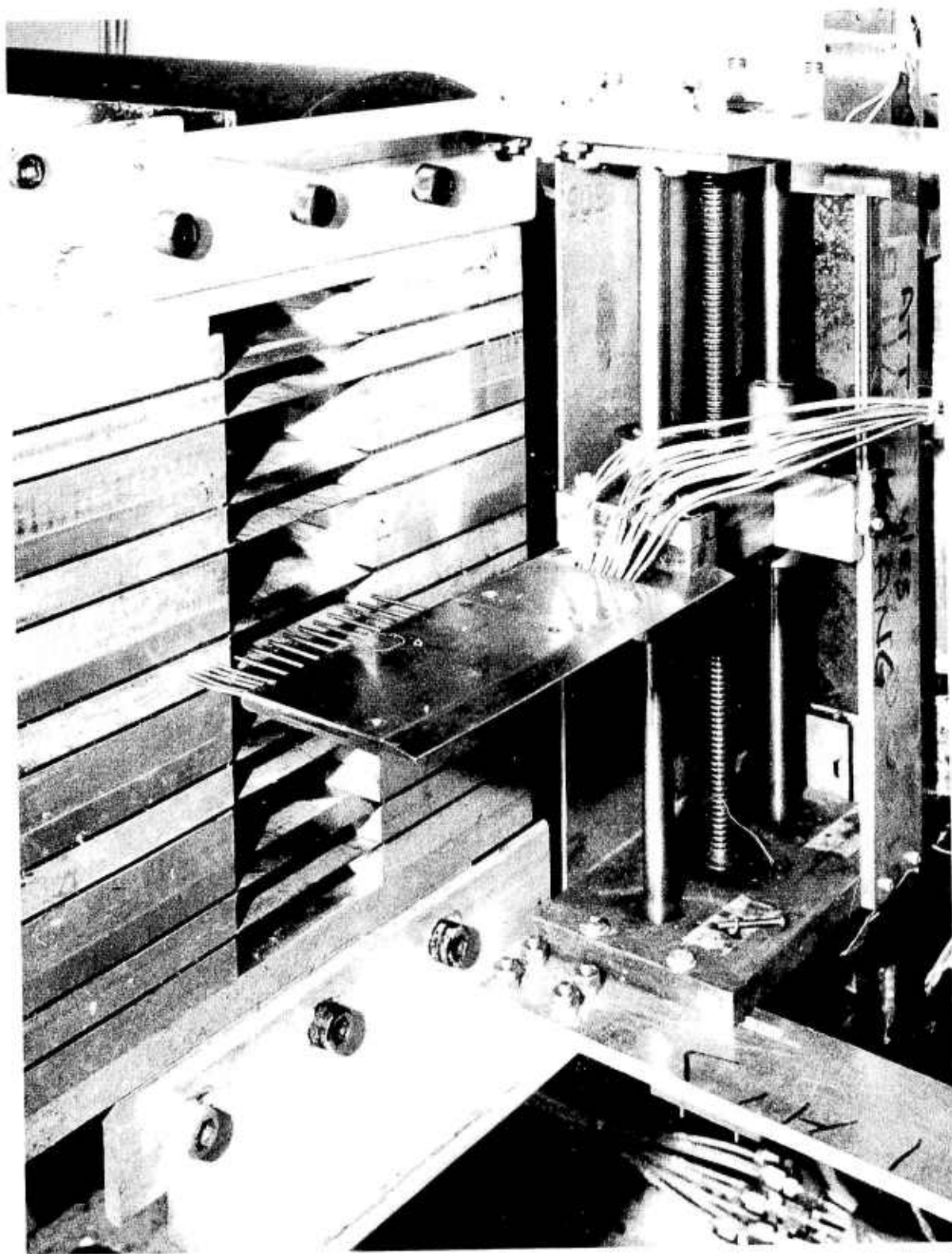


Figure 9. — Location of Primary and Secondary Plenum Pressure Ports



*Figure 10.—Ejector and Primary Nozzle Details*



*Figure 11.—Primary Exit Total Pressure Rake*



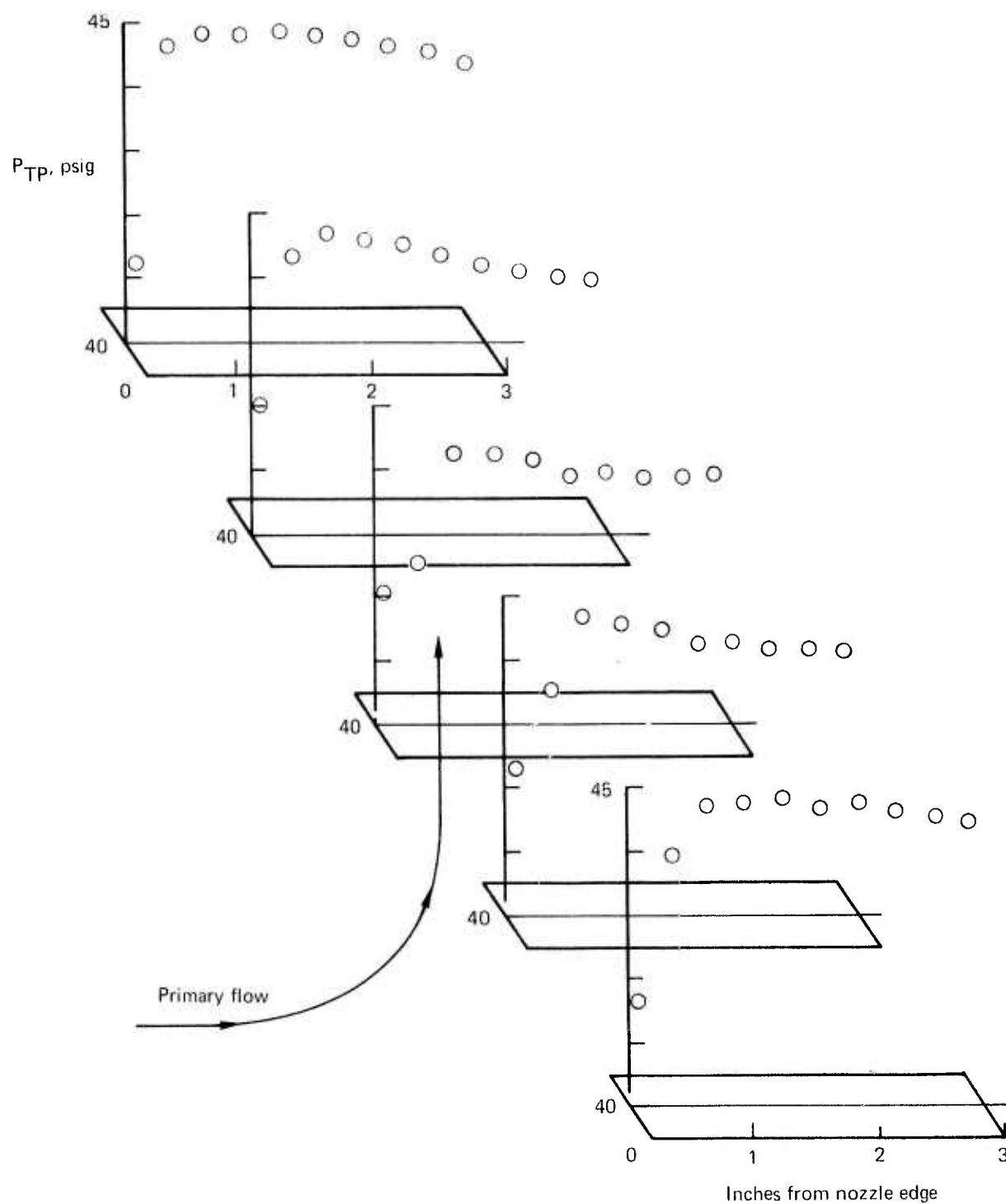


Figure 12.—Total Pressure Survey of Primary Exits ( $P_{TP}/P_{amb} = 4.0$ )

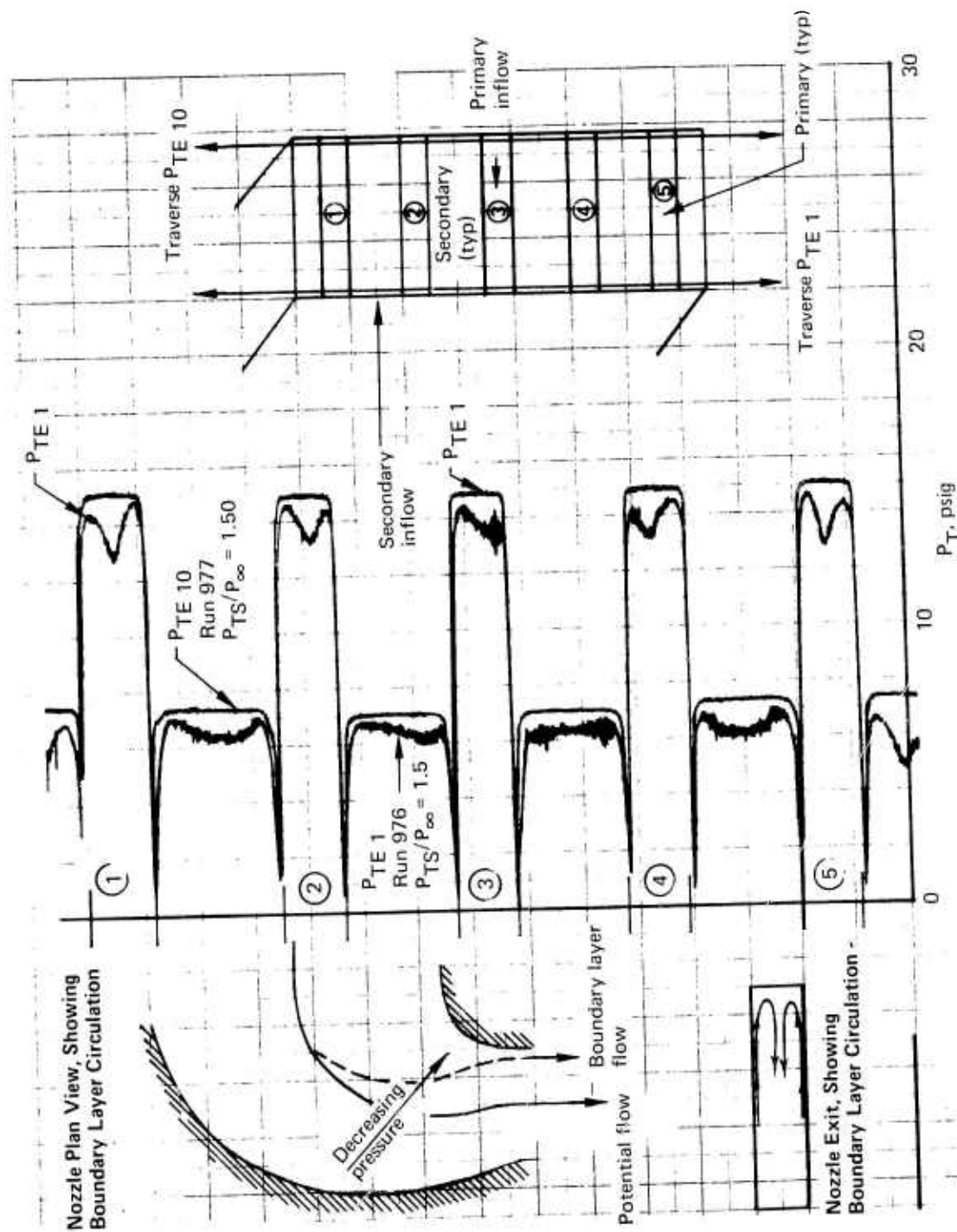


Figure 13.—Total Pressure Profiles, Primary and Secondary Flows, Showing Flow Circulation

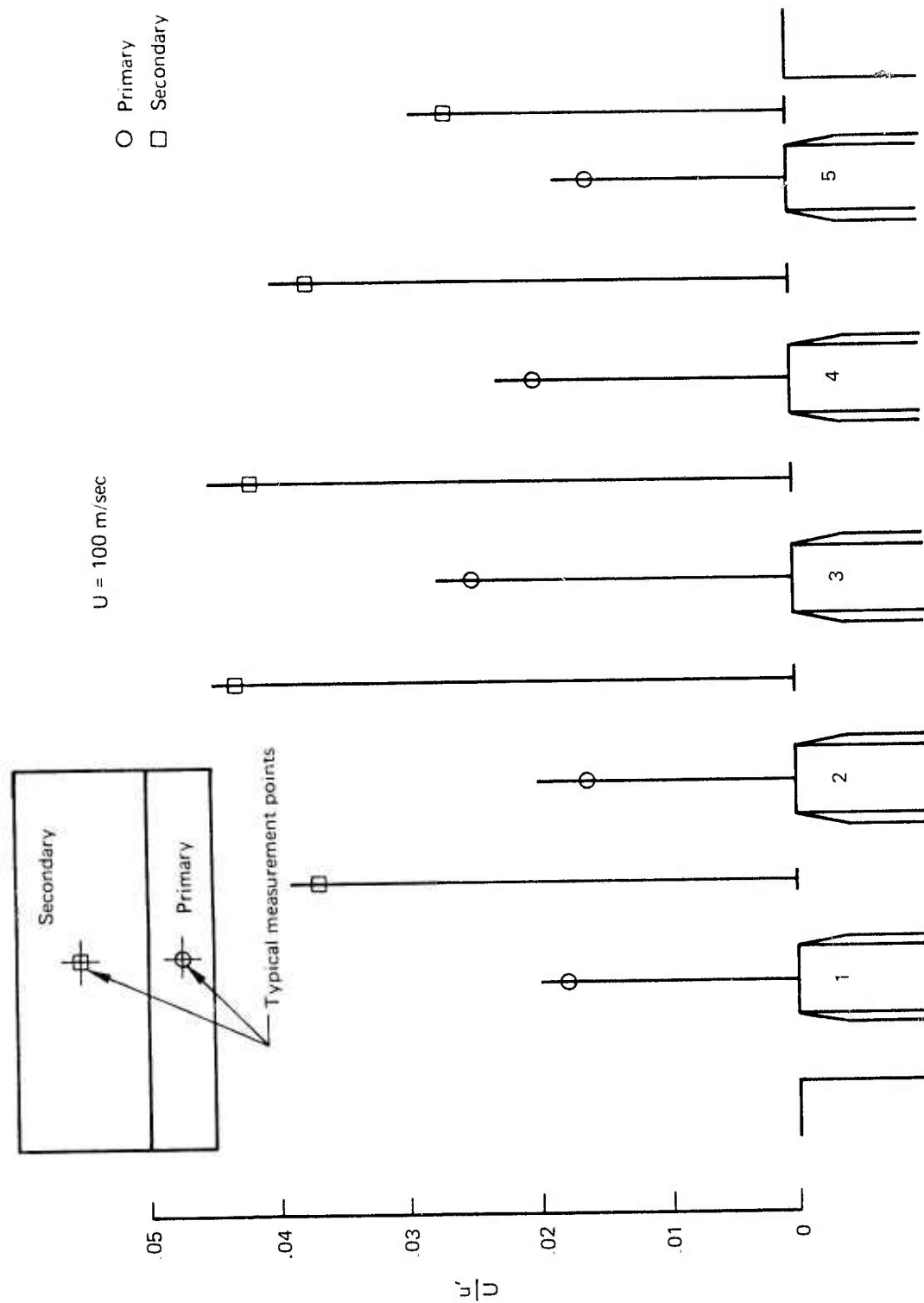


Figure 14. — Turbulence Intensities at Nozzle Centers—Baseline

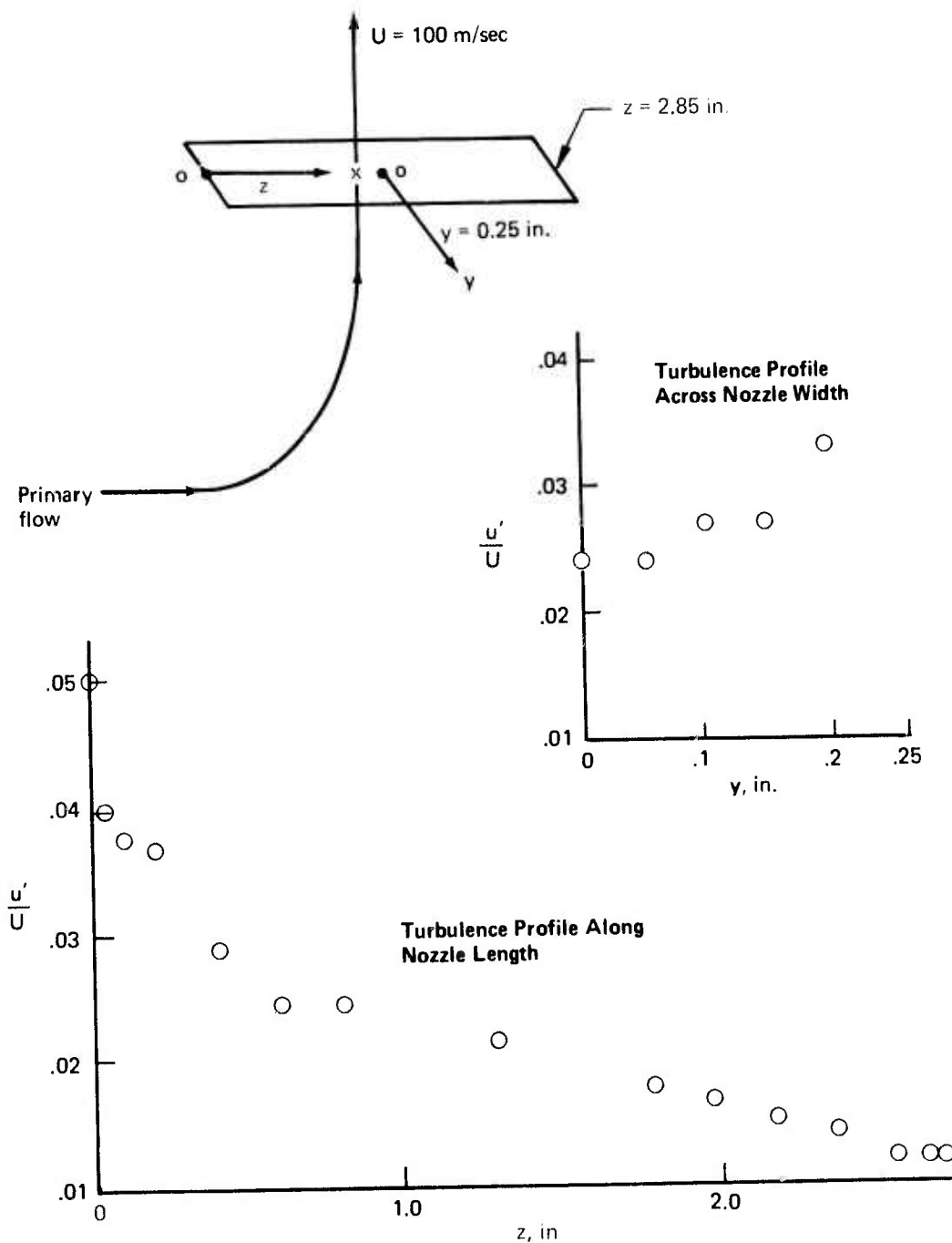


Figure 15.—Primary Nozzle Turbulence Intensity Profiles

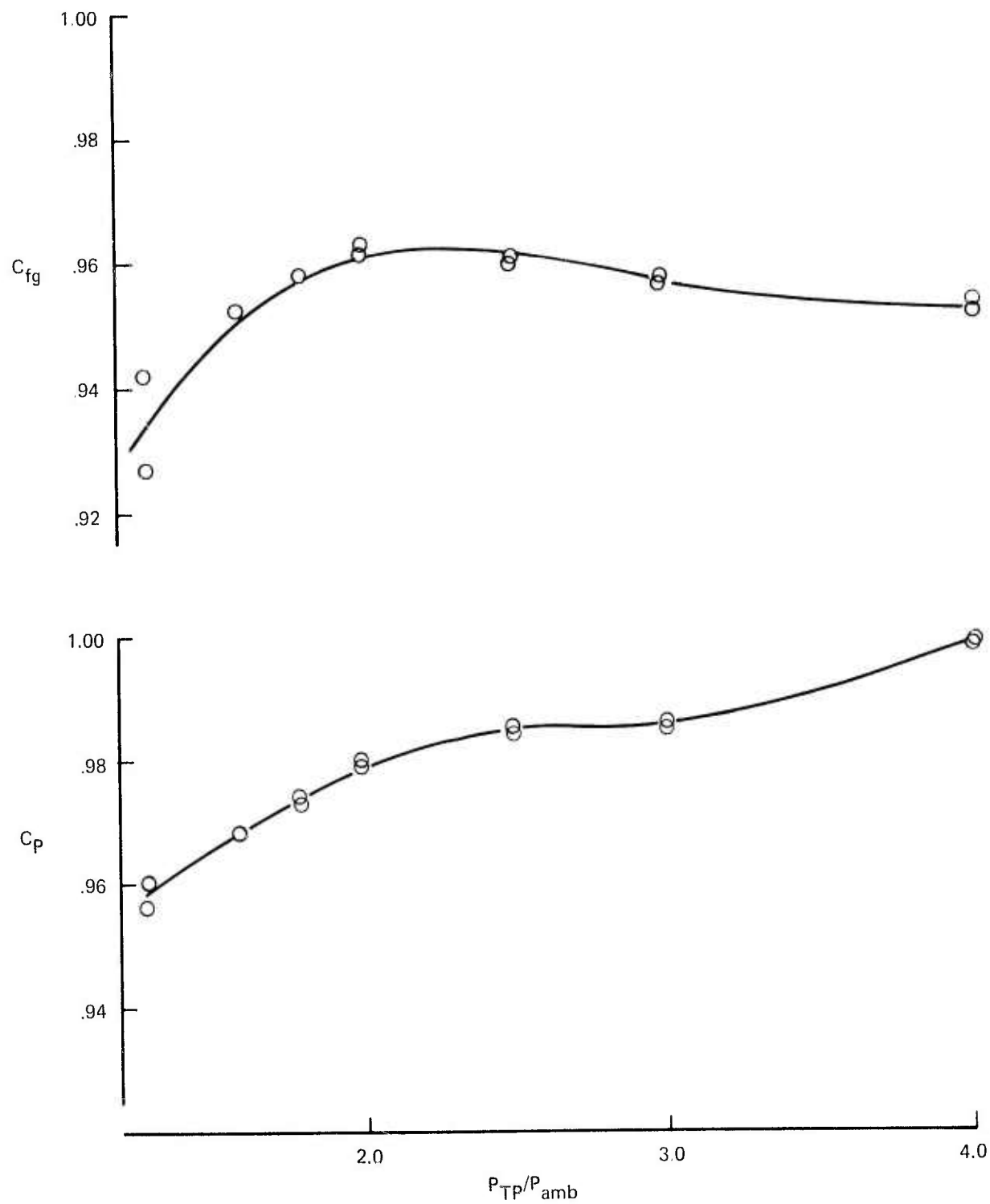


Figure 16.—Baseline Nozzle Performance Without Ejector



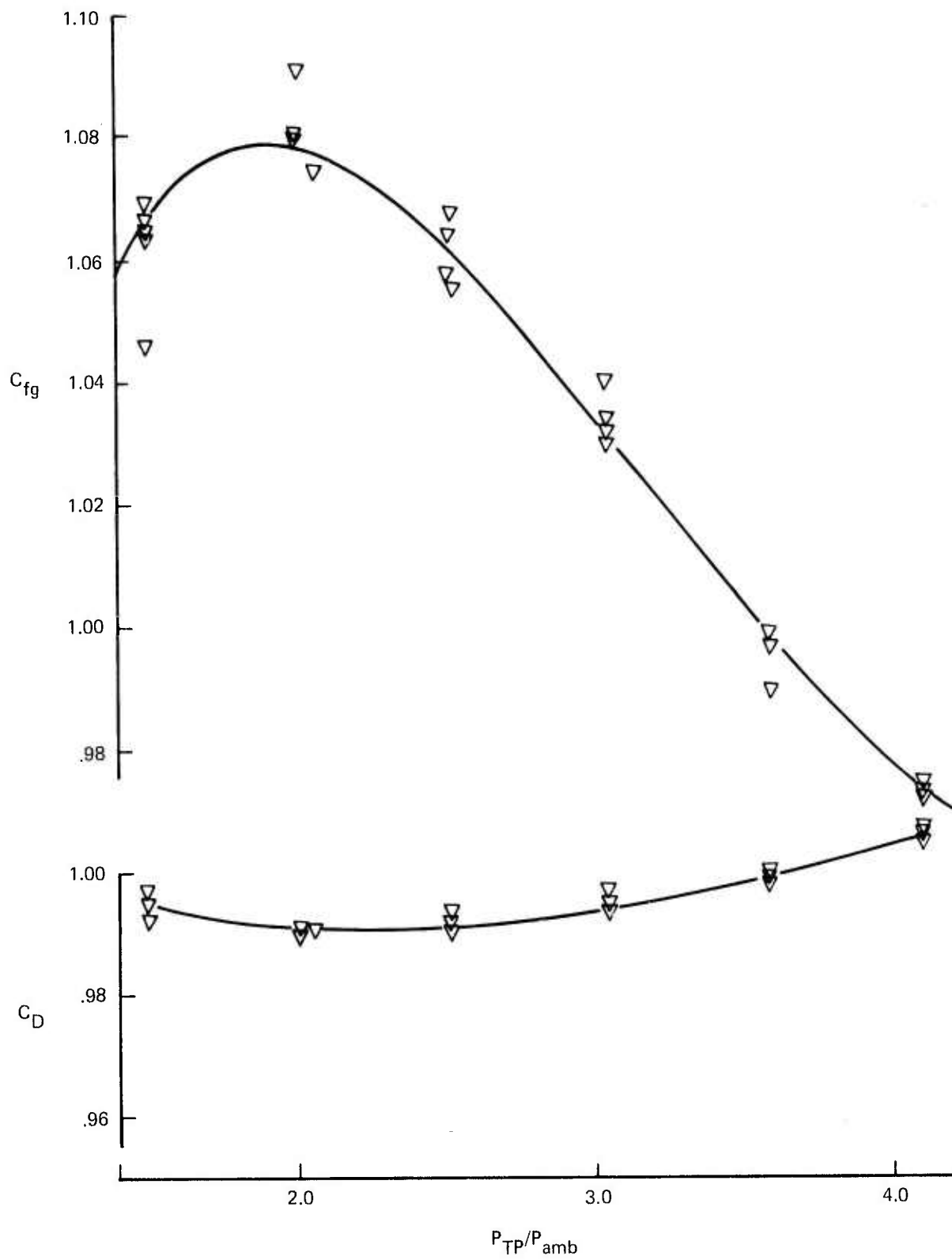


Figure 17.—Baseline Nozzle Performance With Ejector

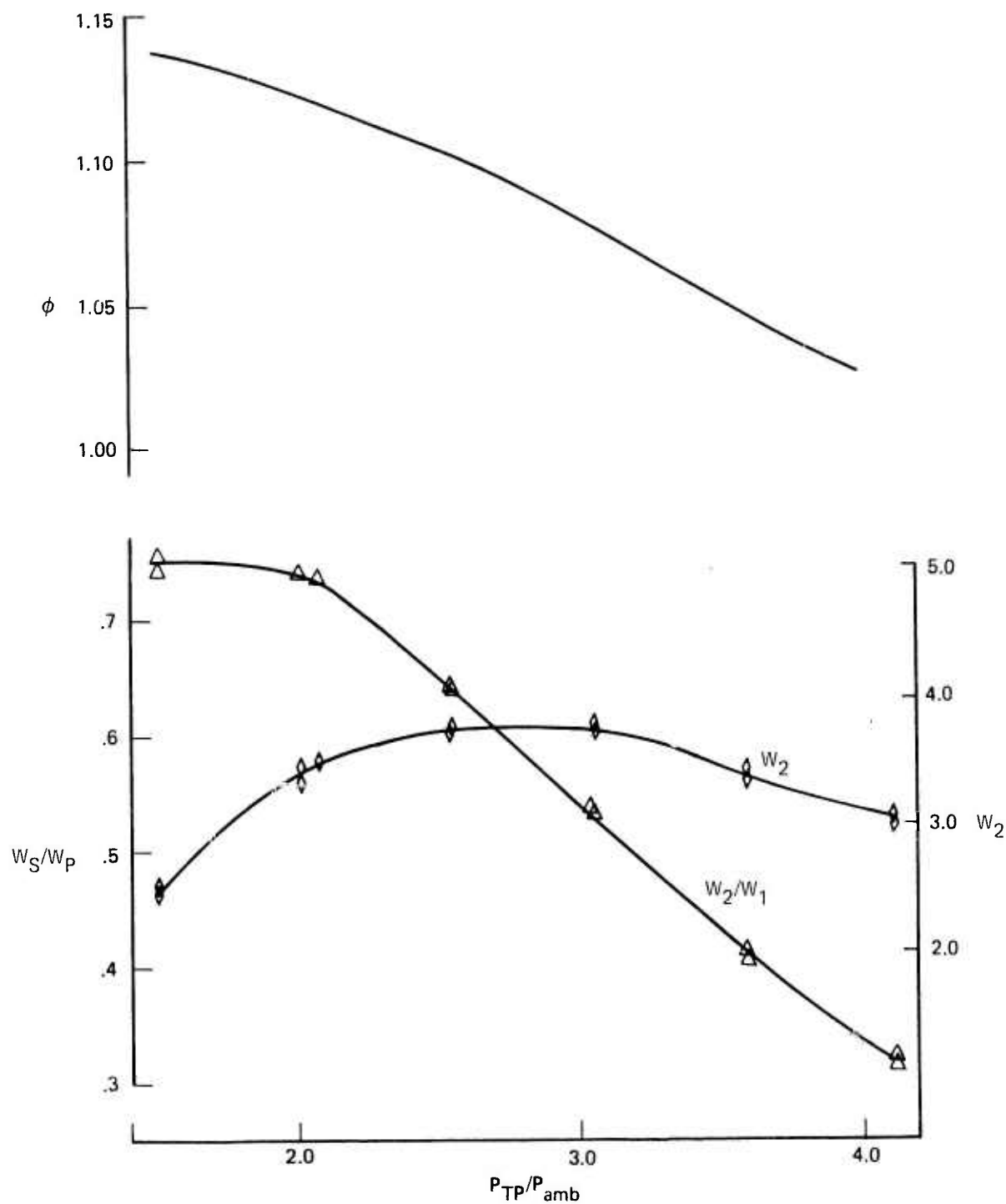


Figure 13.—Baseline Nozzle With Ejector, Secondary Weight Flow, Thrust, and Weight Flow Augmentation

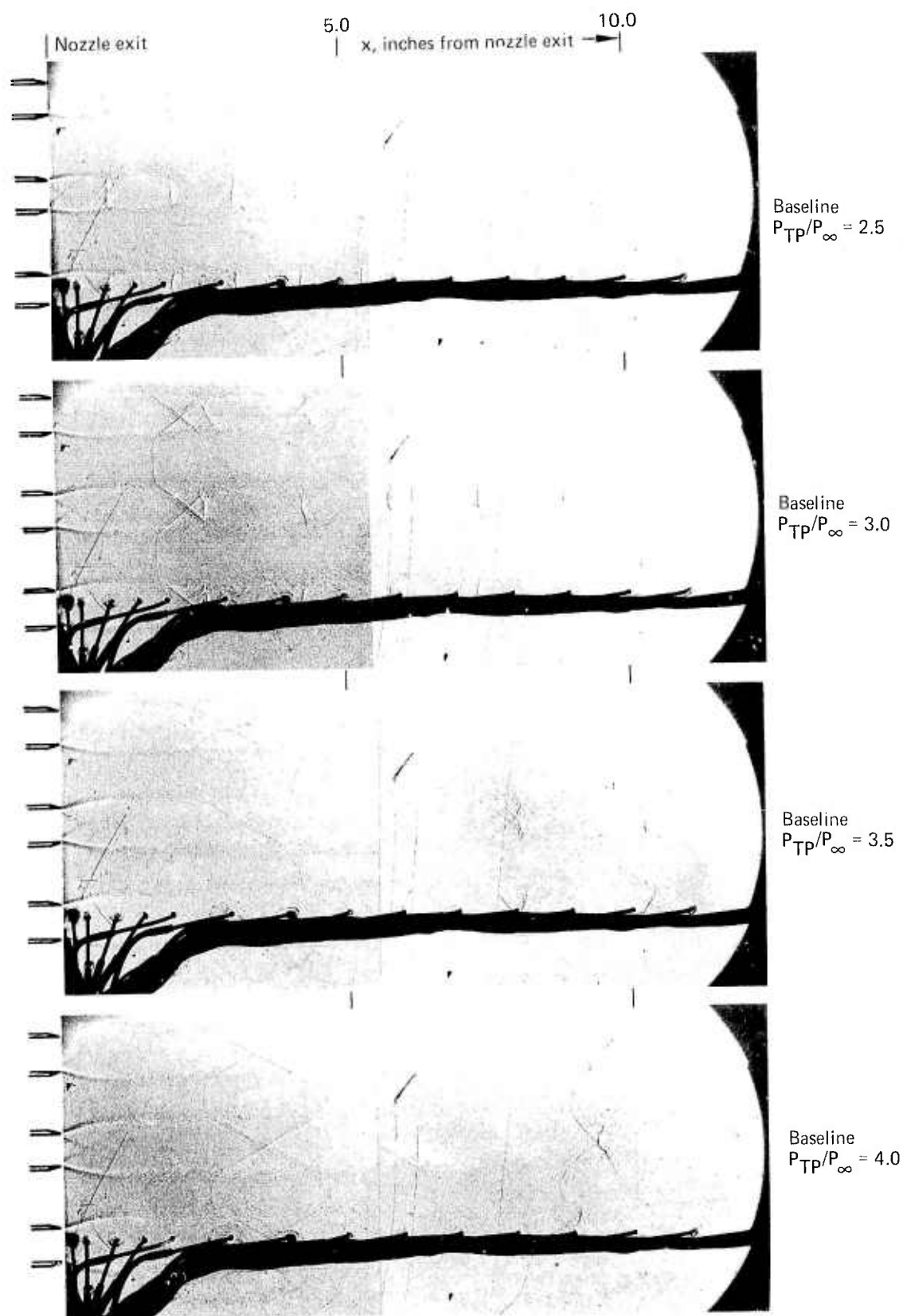


Figure 19.—Spark Shadowgraph Photos of Baseline Nozzle With Ejector

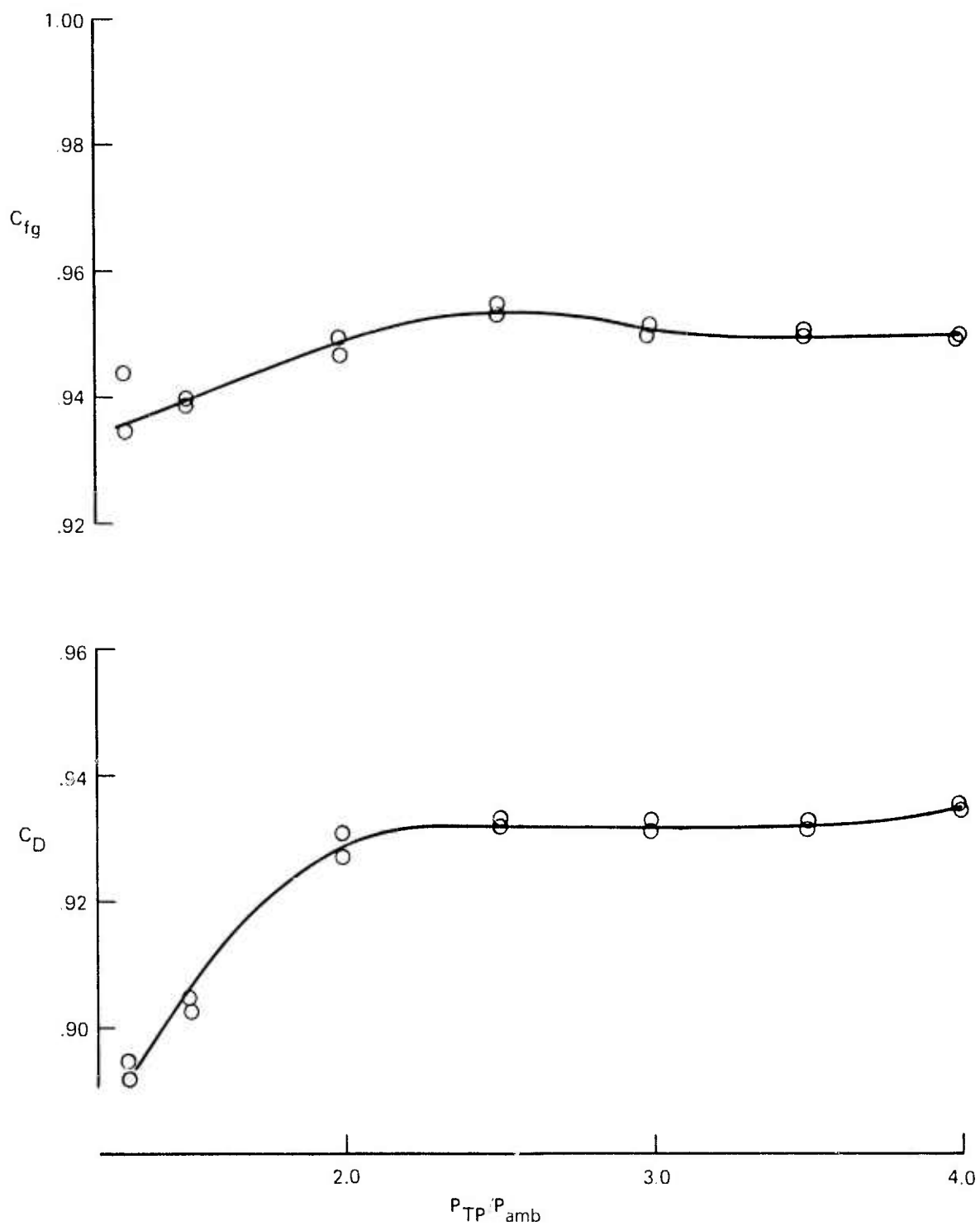


Figure 20.—Long Throat Nozzle Performance Without Ejector

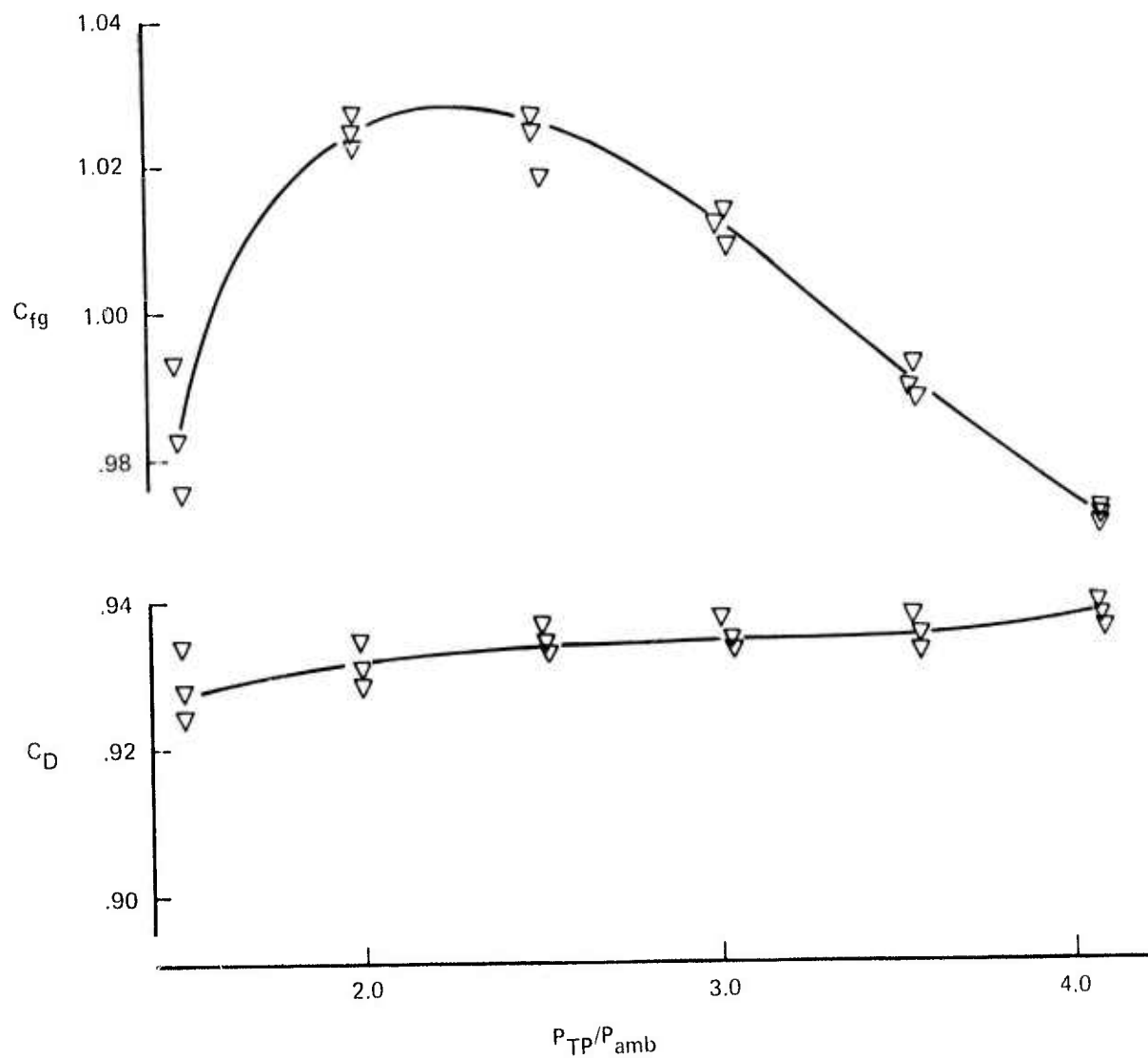


Figure 21.—Long Throat Nozzle Performance With Ejector



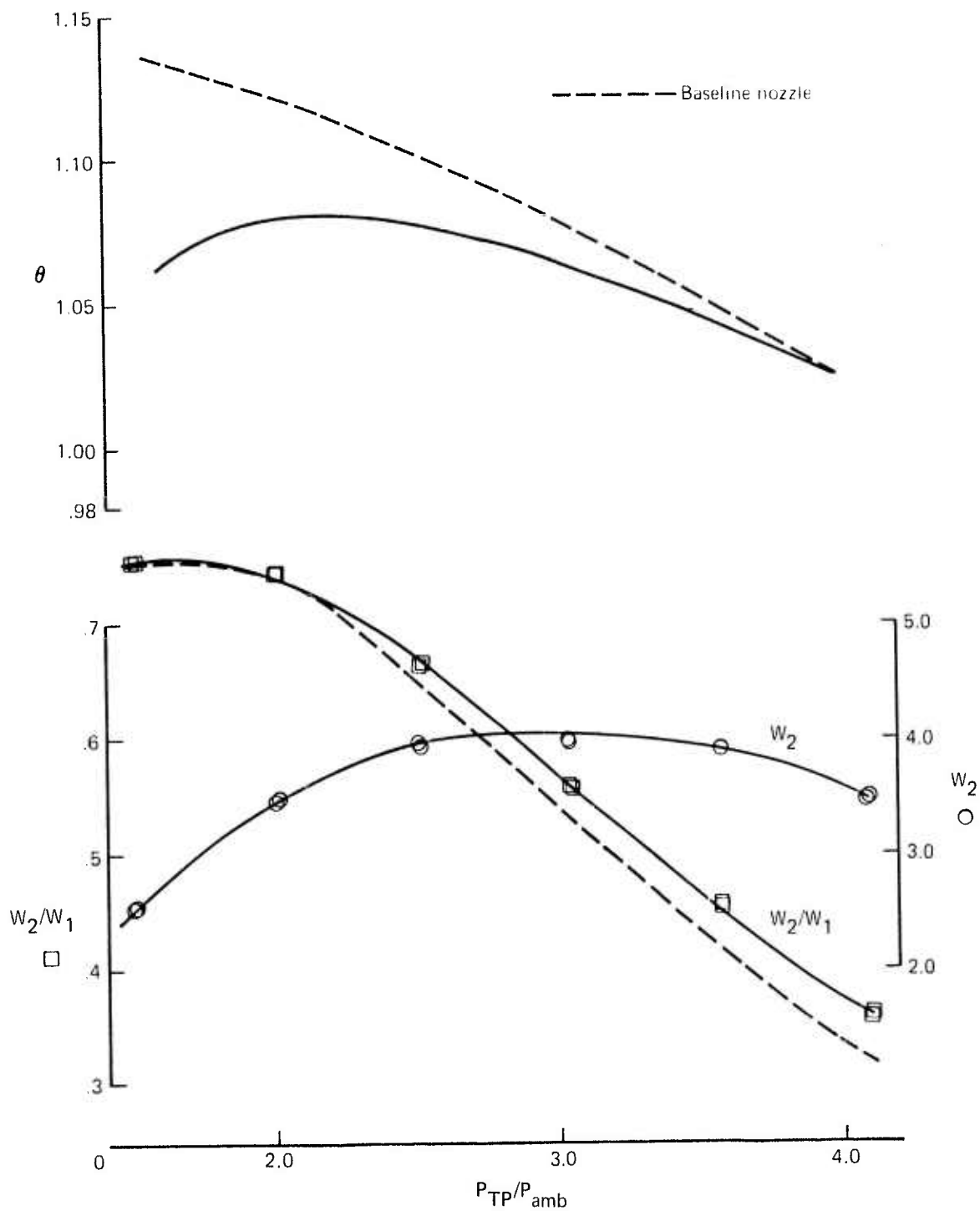


Figure 22.—Long Throat Nozzle With Ejector, Secondary Weight Flow, Thrust, and Weight Flow Augmentation

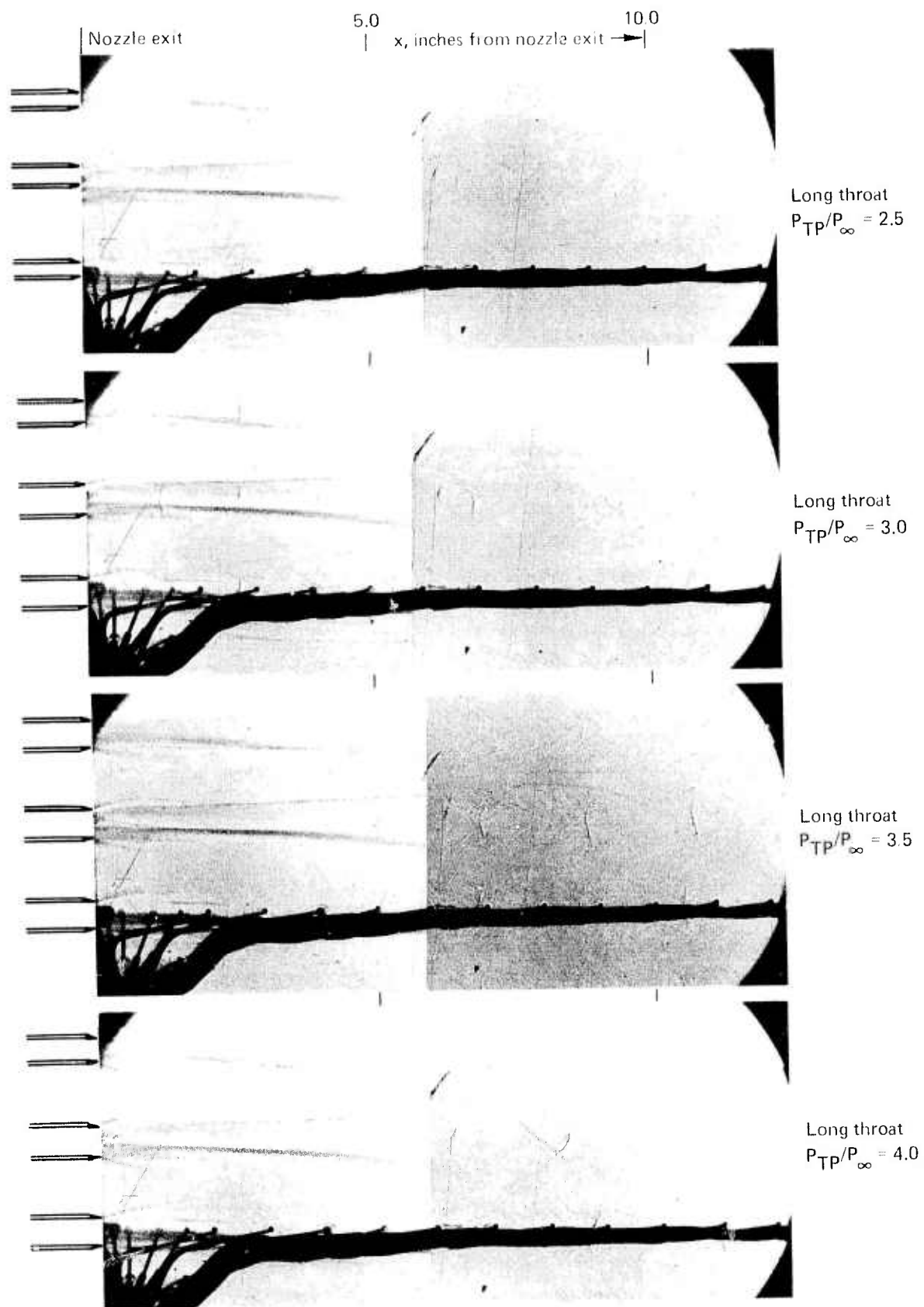


Figure 23.—Spark Shadowgraph Photos of Long Throat Nozzle With Ejector

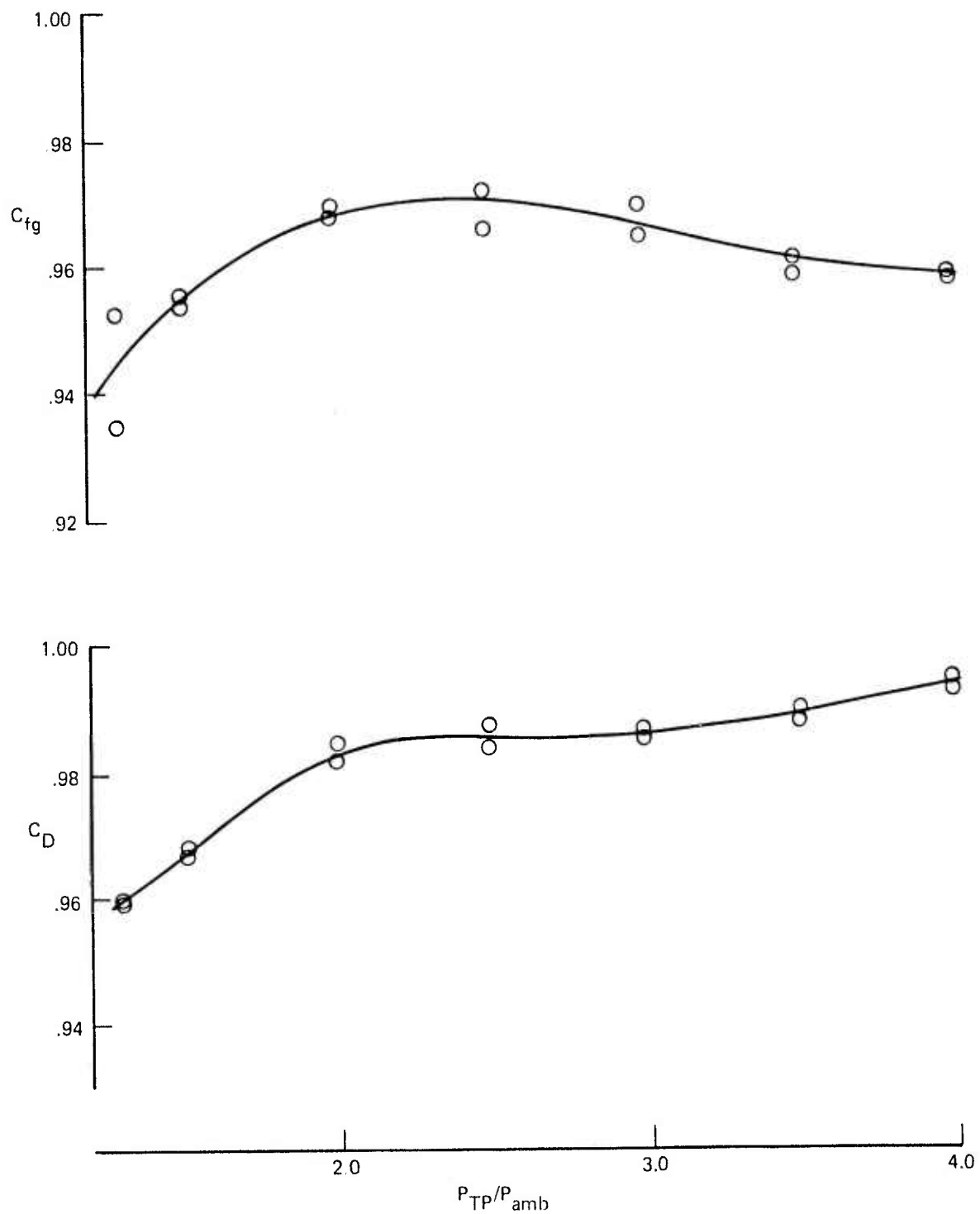


Figure 24.—Thick Base Nozzle Performance Without Ejector

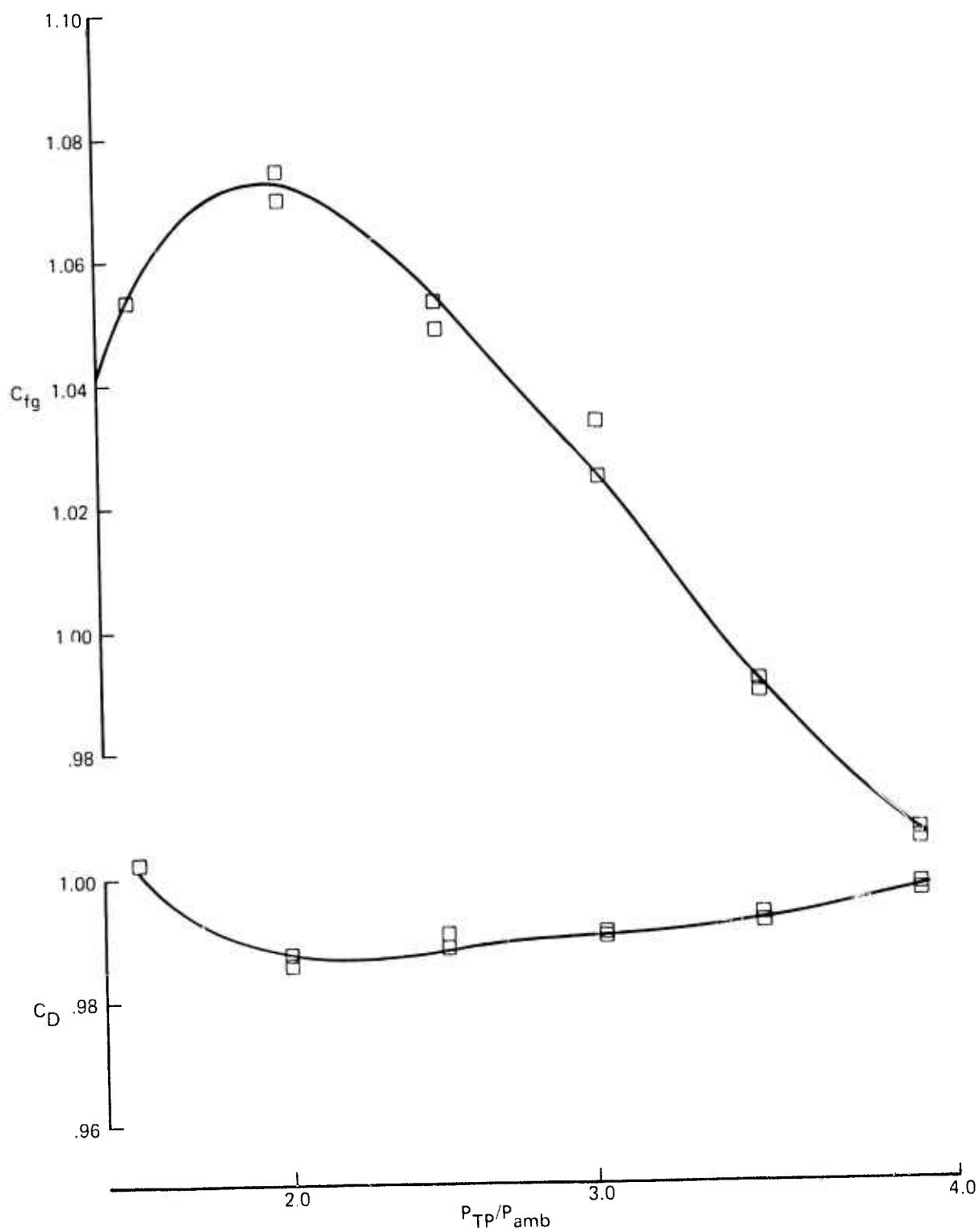


Figure 25.—Thick Base Nozzle Performance With Ejector

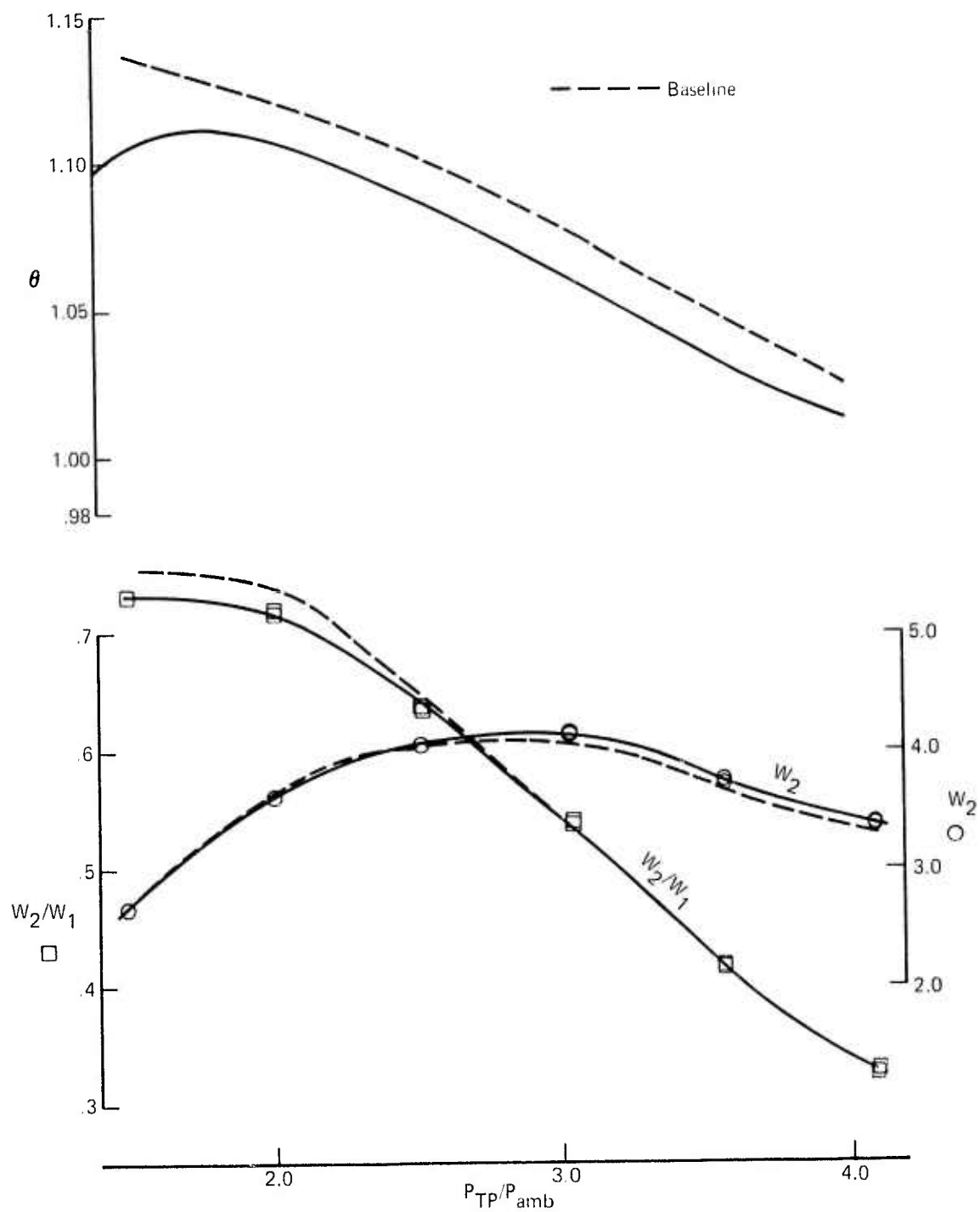


Figure 26. —Thick Base Nozzle With Ejector, Secondary Weight Flow, Thrust, and Weight Flow Augmentation



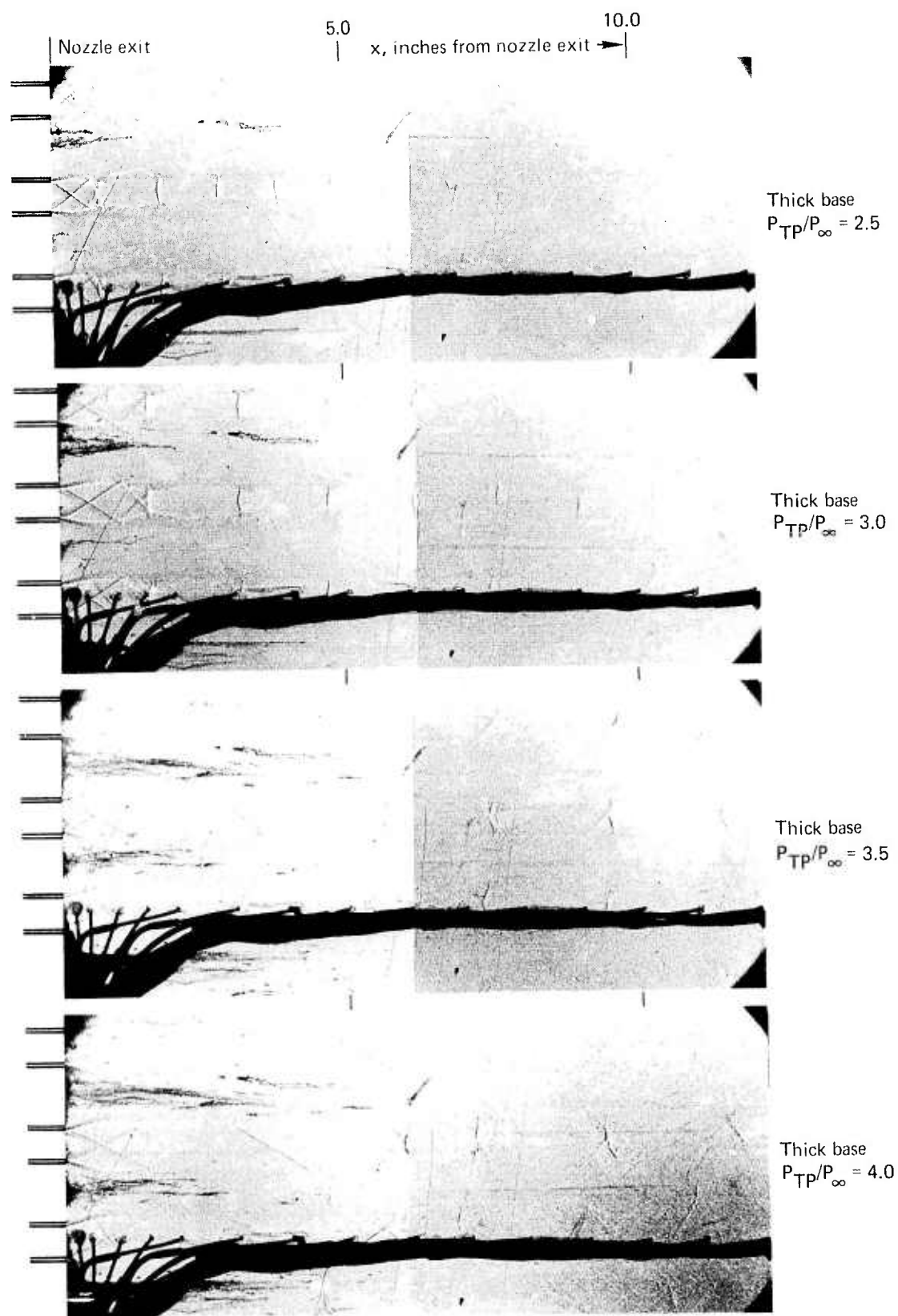


Figure 27.—Spark Shadowgraph Photos of Thick Base Nozzle With Ejector

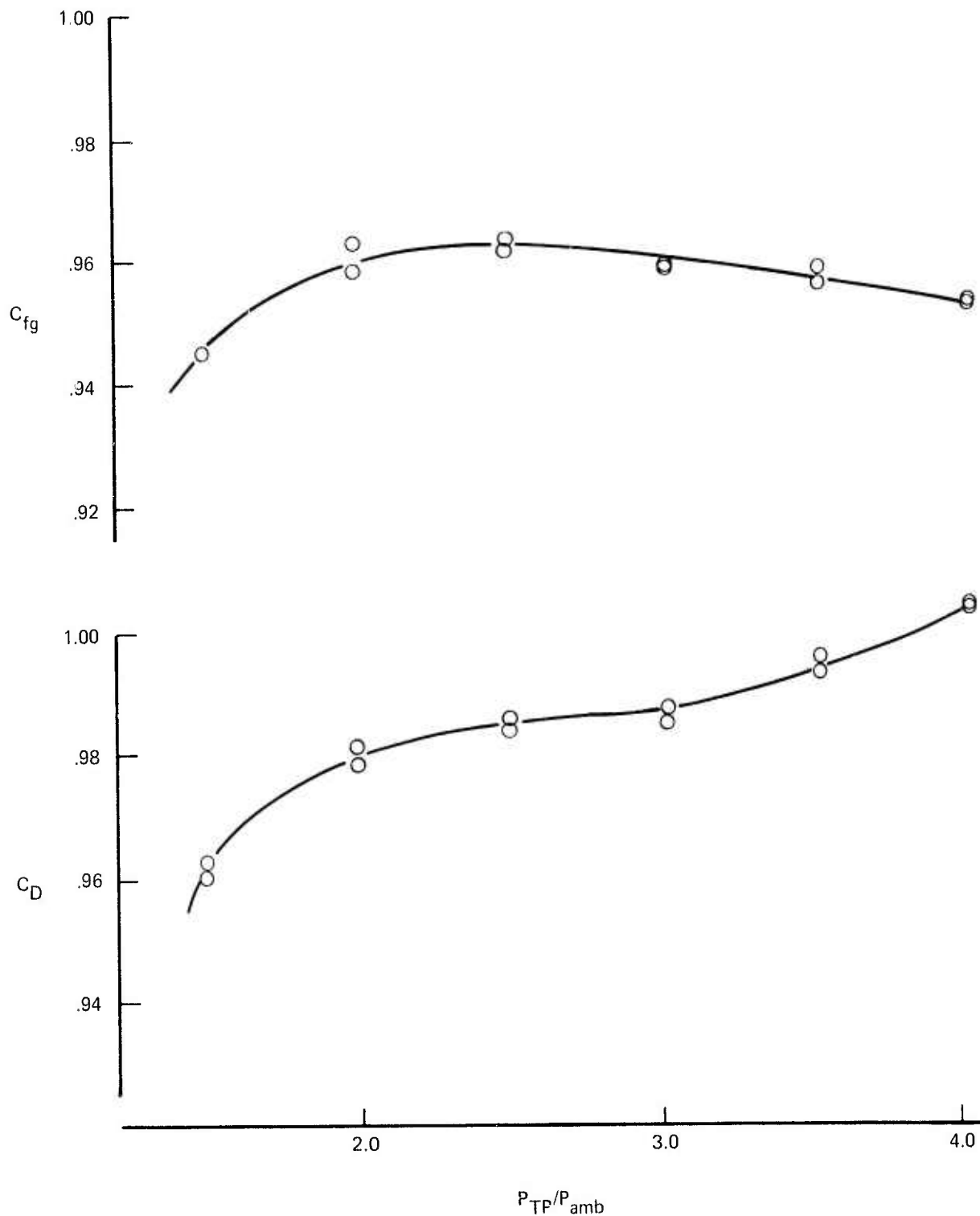


Figure 28.—High Turbulence Nozzle Performance Without Ejector

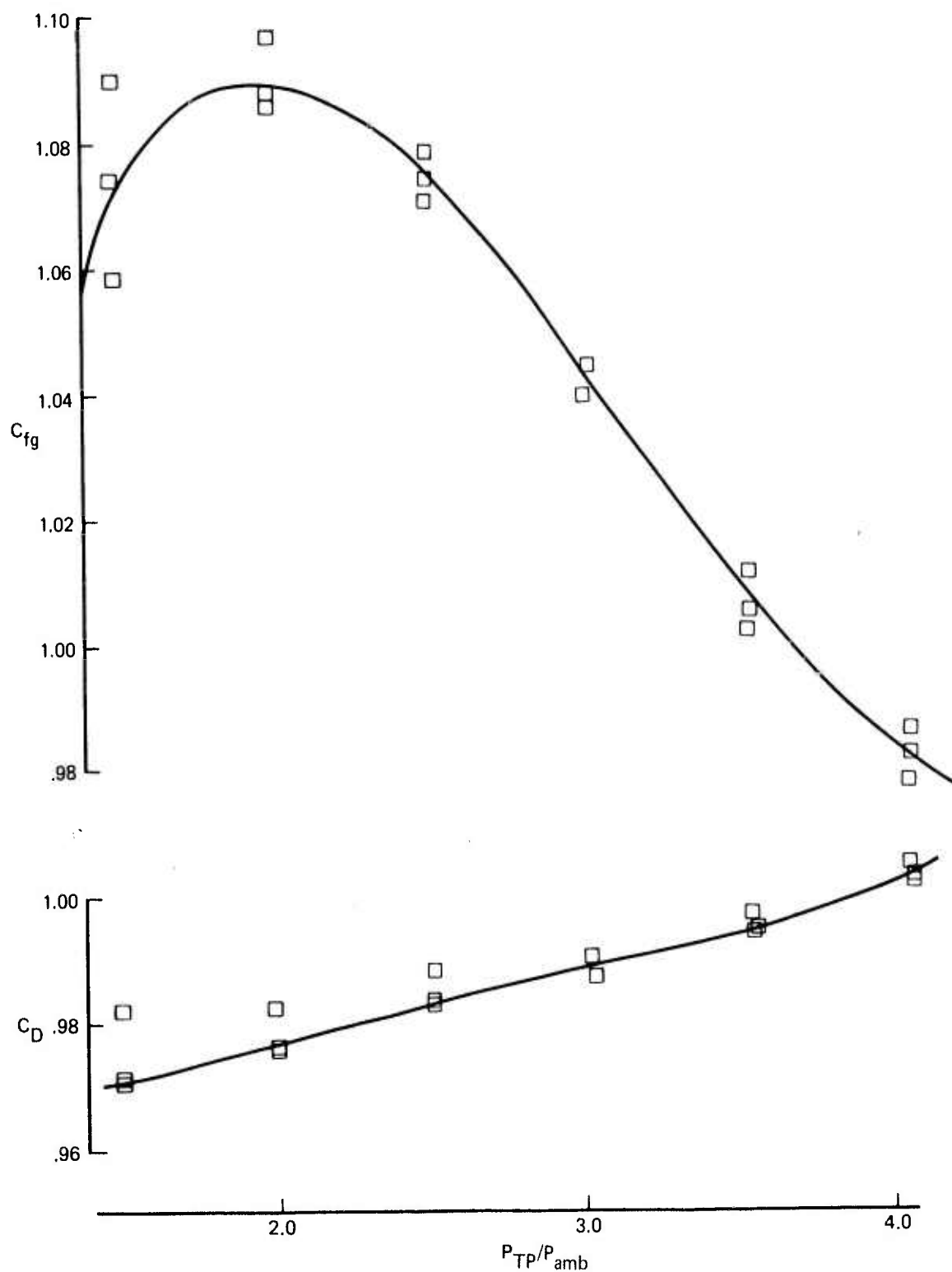


Figure 29.—High Turbulence Nozzle Performance With Ejector

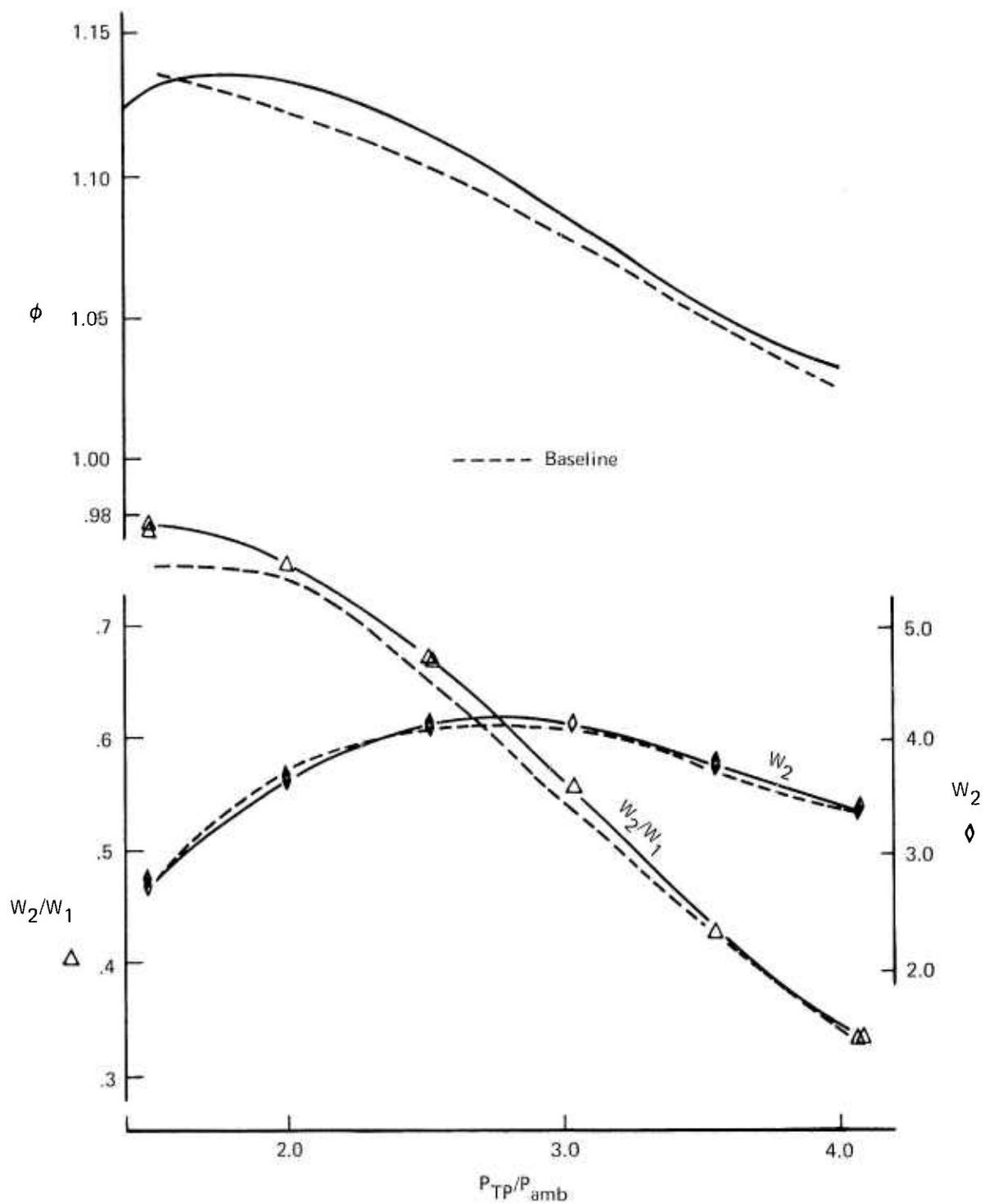


Figure 30.—High Turbulence Nozzle With Ejector, Secondary Weight Flow, Thrust, and Weight Flow Augmentation

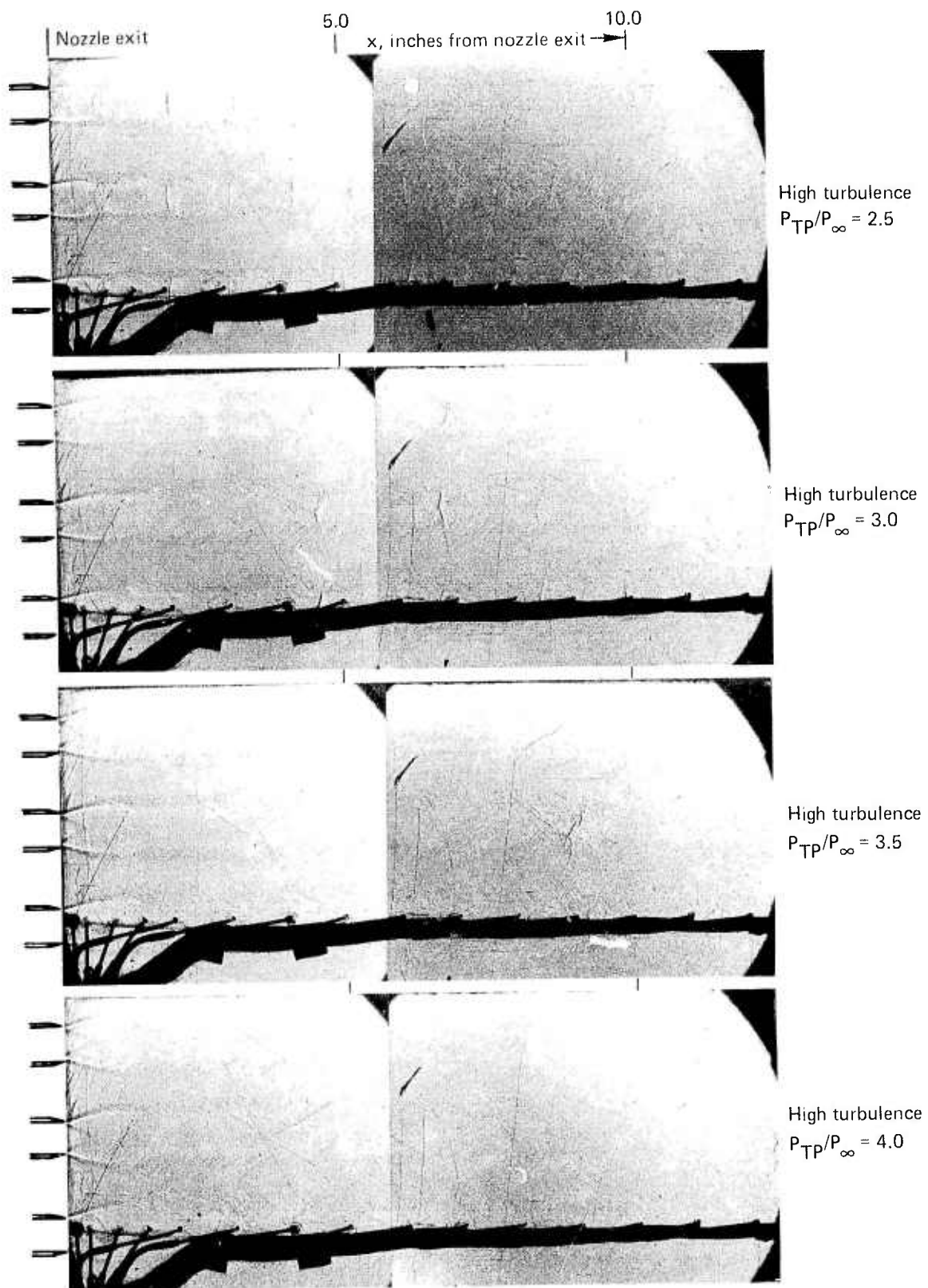


Figure 31.—Spark Shadowgraph Photos of High Turbulence Nozzle With Ejector



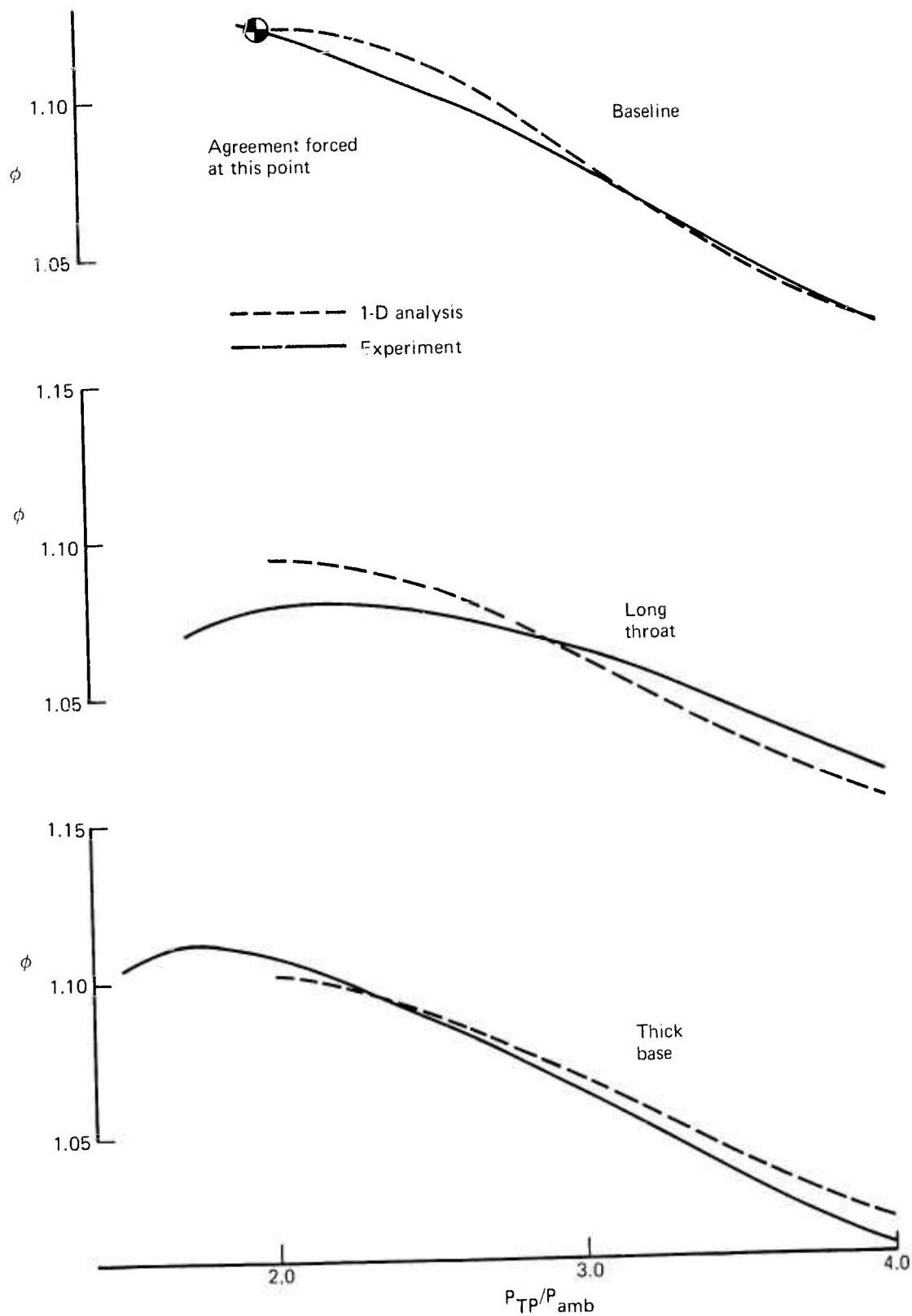


Figure 32.—Comparison of Experimentally and Analytically Determined Augmentation Ratios

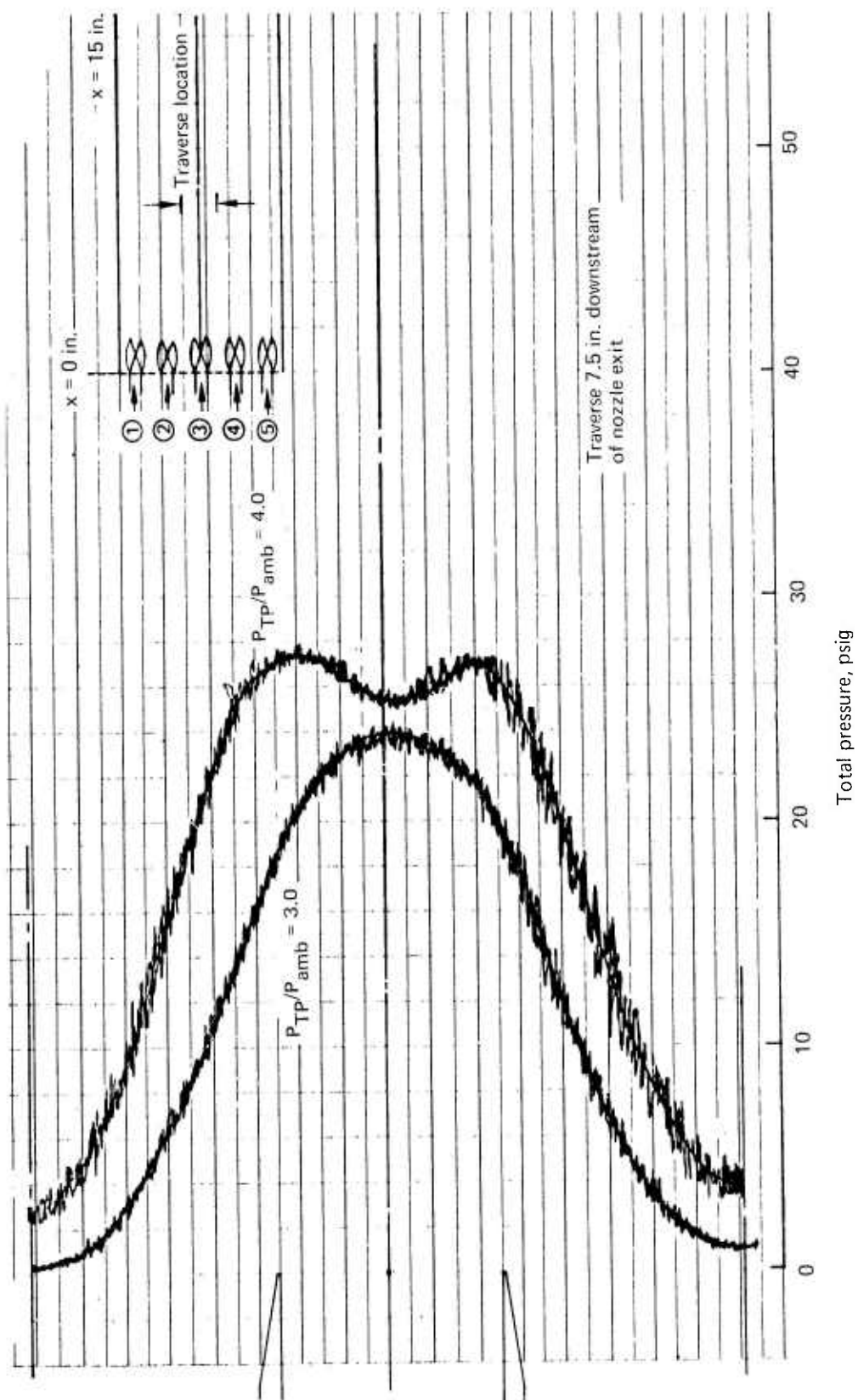


Figure 33.—Typical Total Pressure Profiles

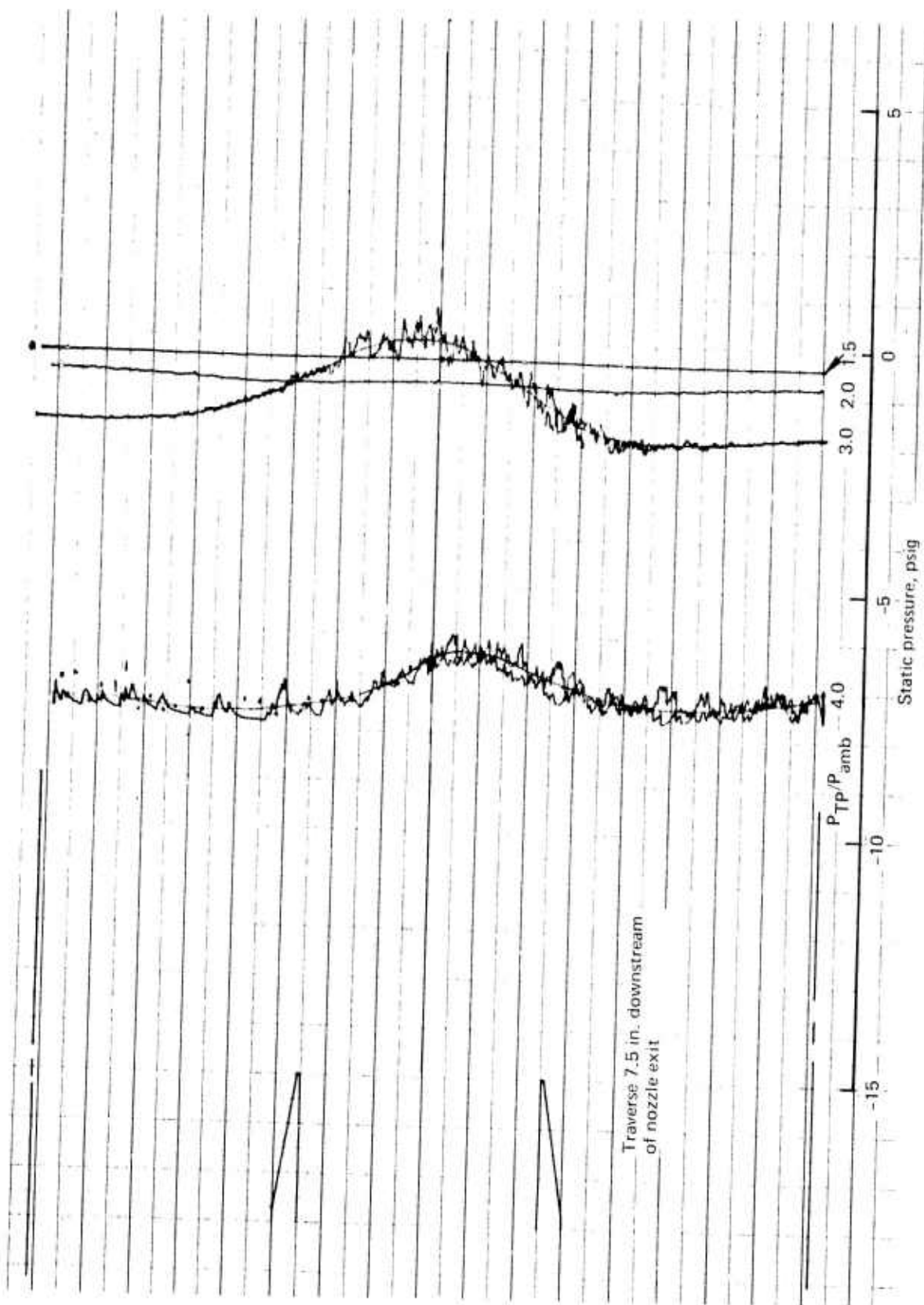


Figure 34. - Typical Static Pressure Profiles

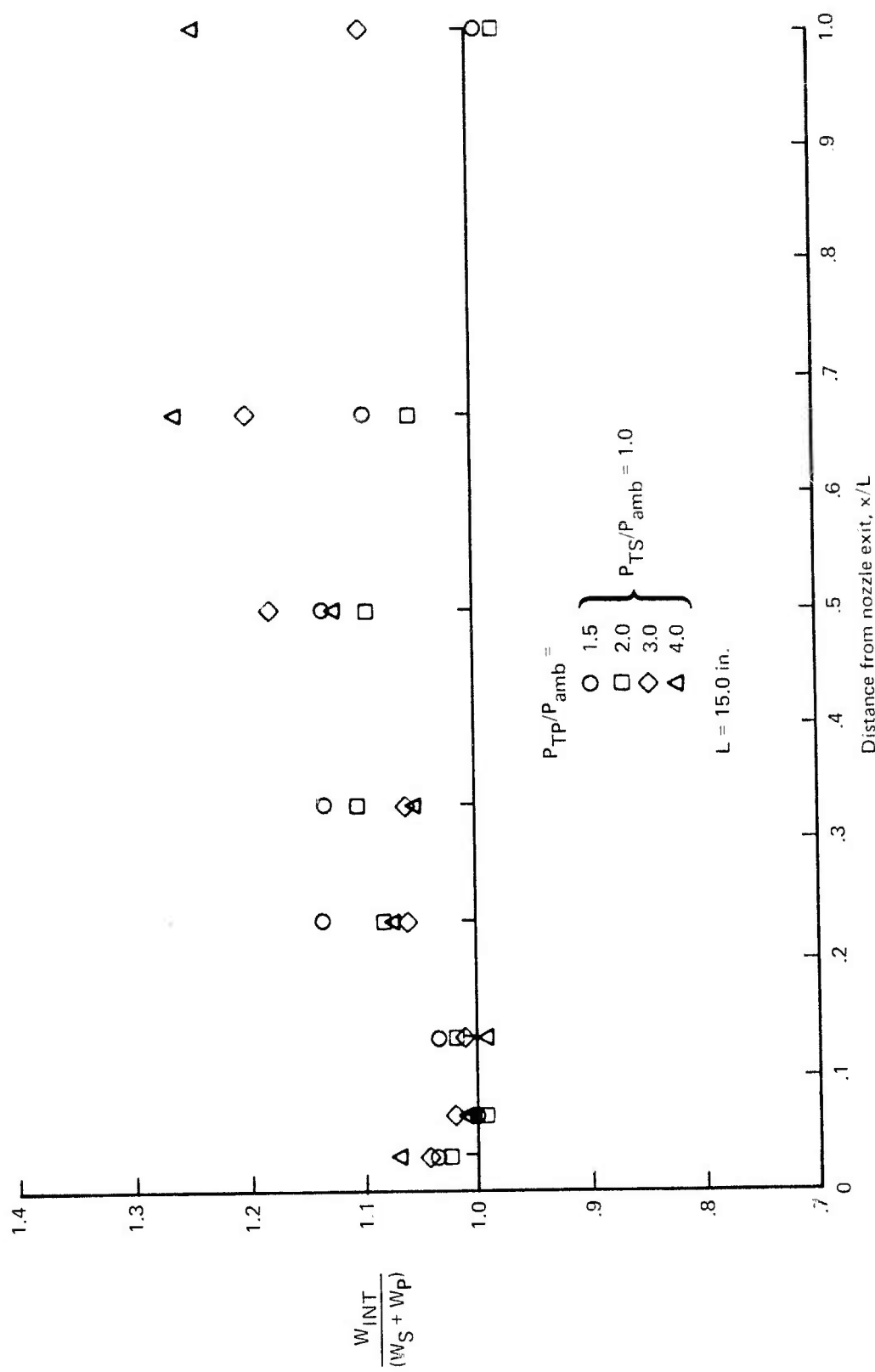


Figure 35.—Profile Integrated Weight Flow Compared With Actual Values—Baseline Nozzle

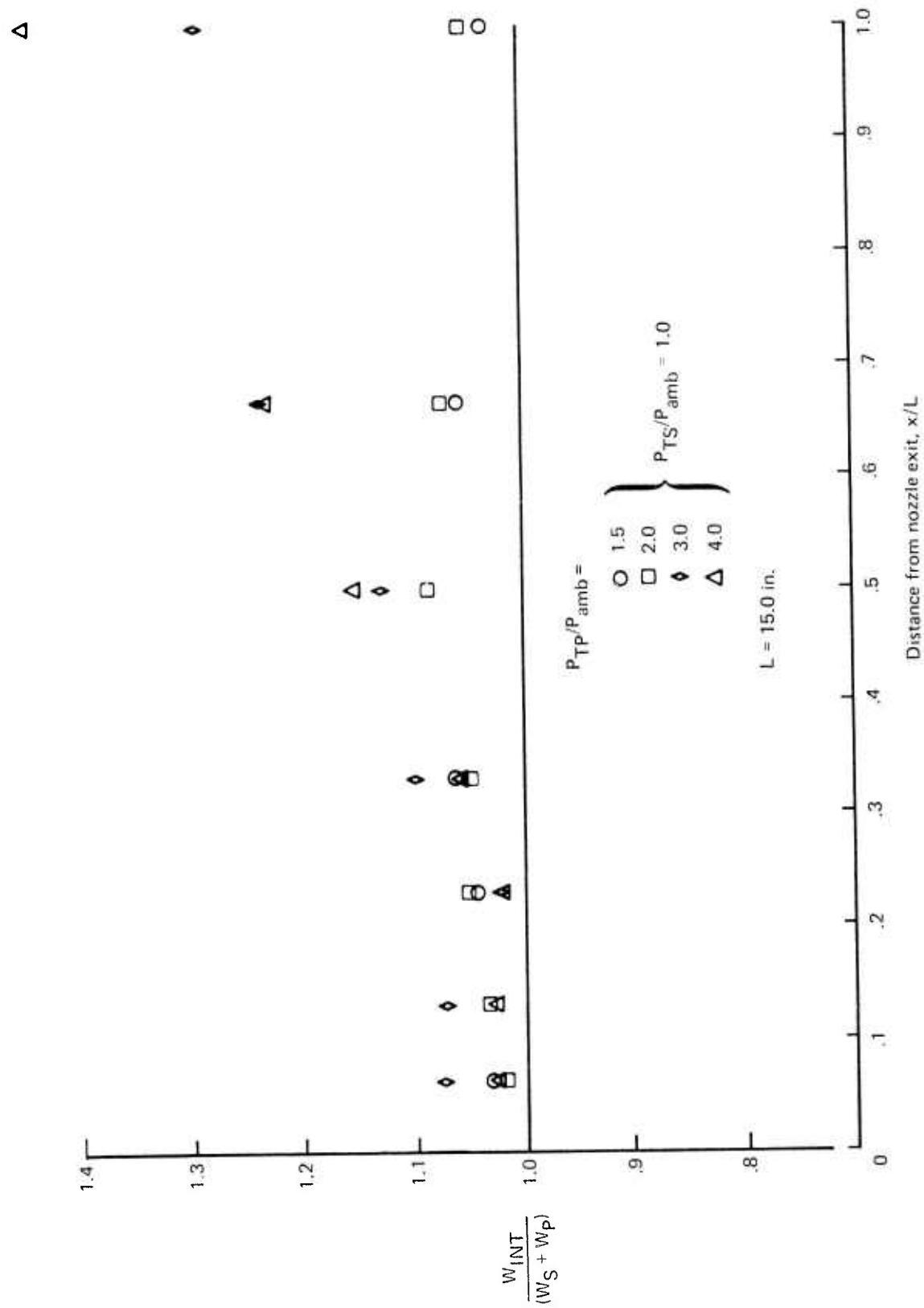


Figure 36. — Profile Integrated Weight Flow Compared With Actual Values—Long Throat Nozzle



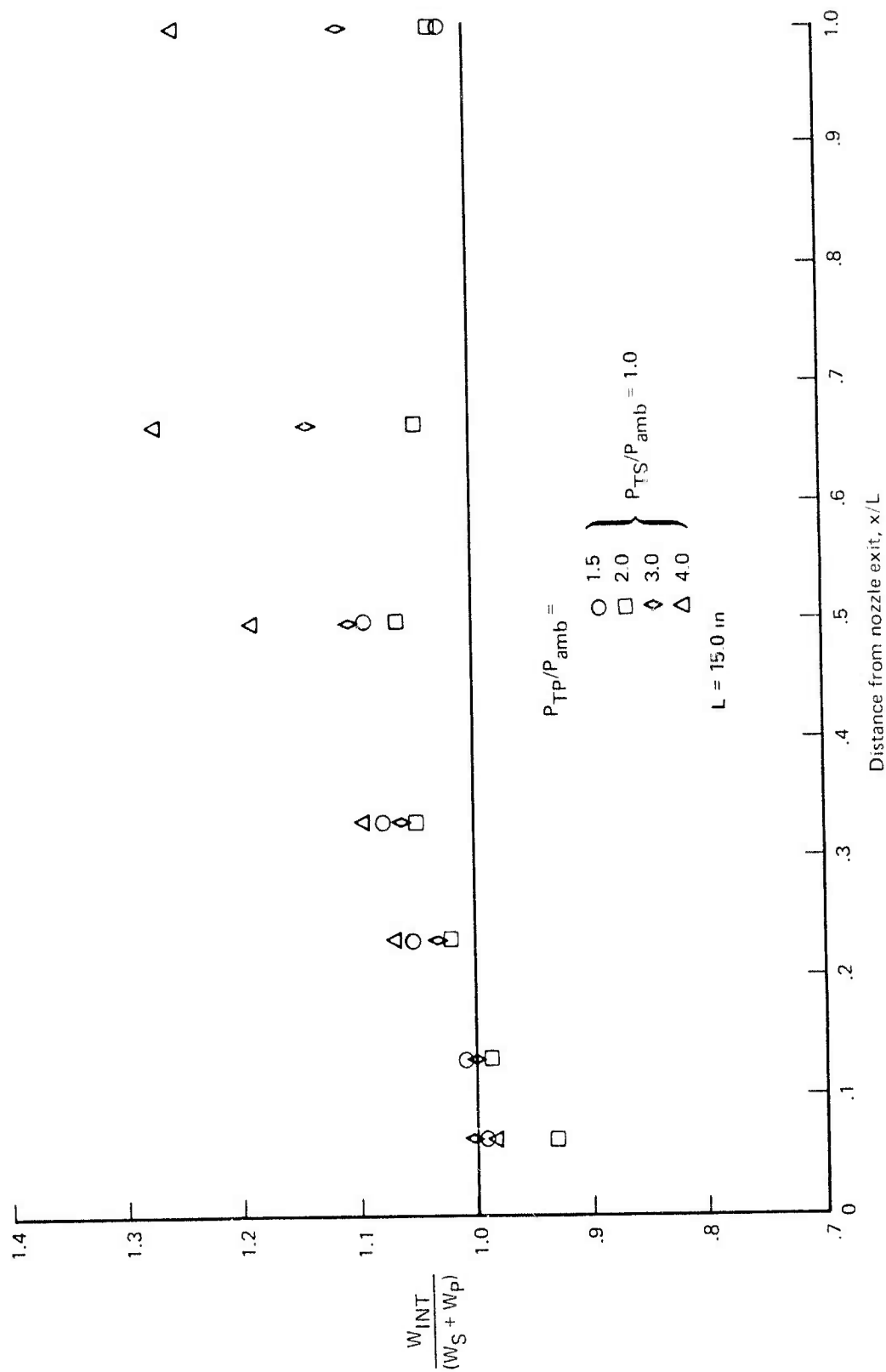


Figure 37.—Profile Integrated Weight Flow Compared With Actual Values—  
Thick Base Nozzle

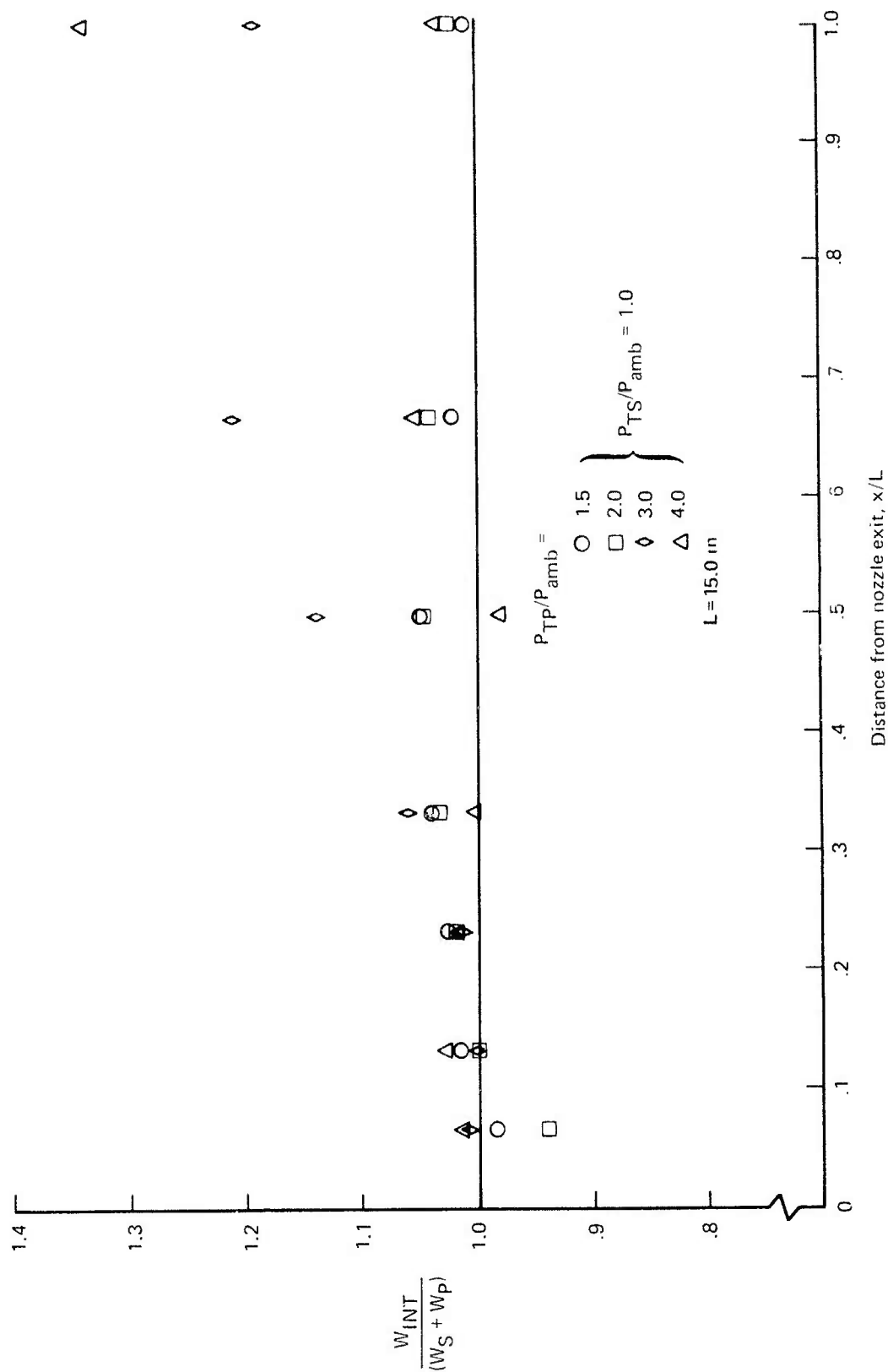


Figure 38.—Profile Integrated Weight Flow Compared With Actual Values—  
High Turbulence Nozzle

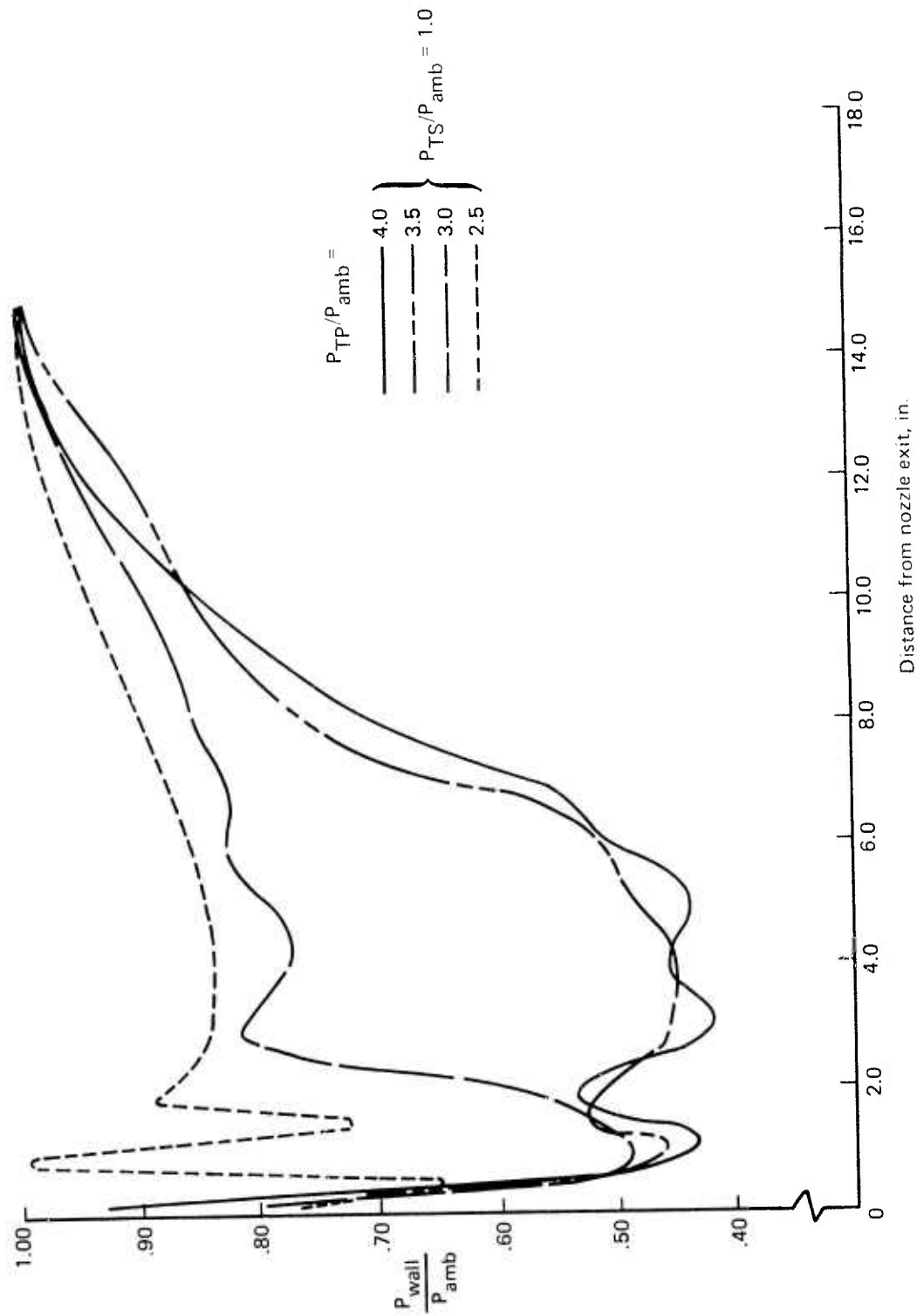


Figure 39.—Axial Static Pressure Distribution on Ejector Sidewall—Baseline Nozzle

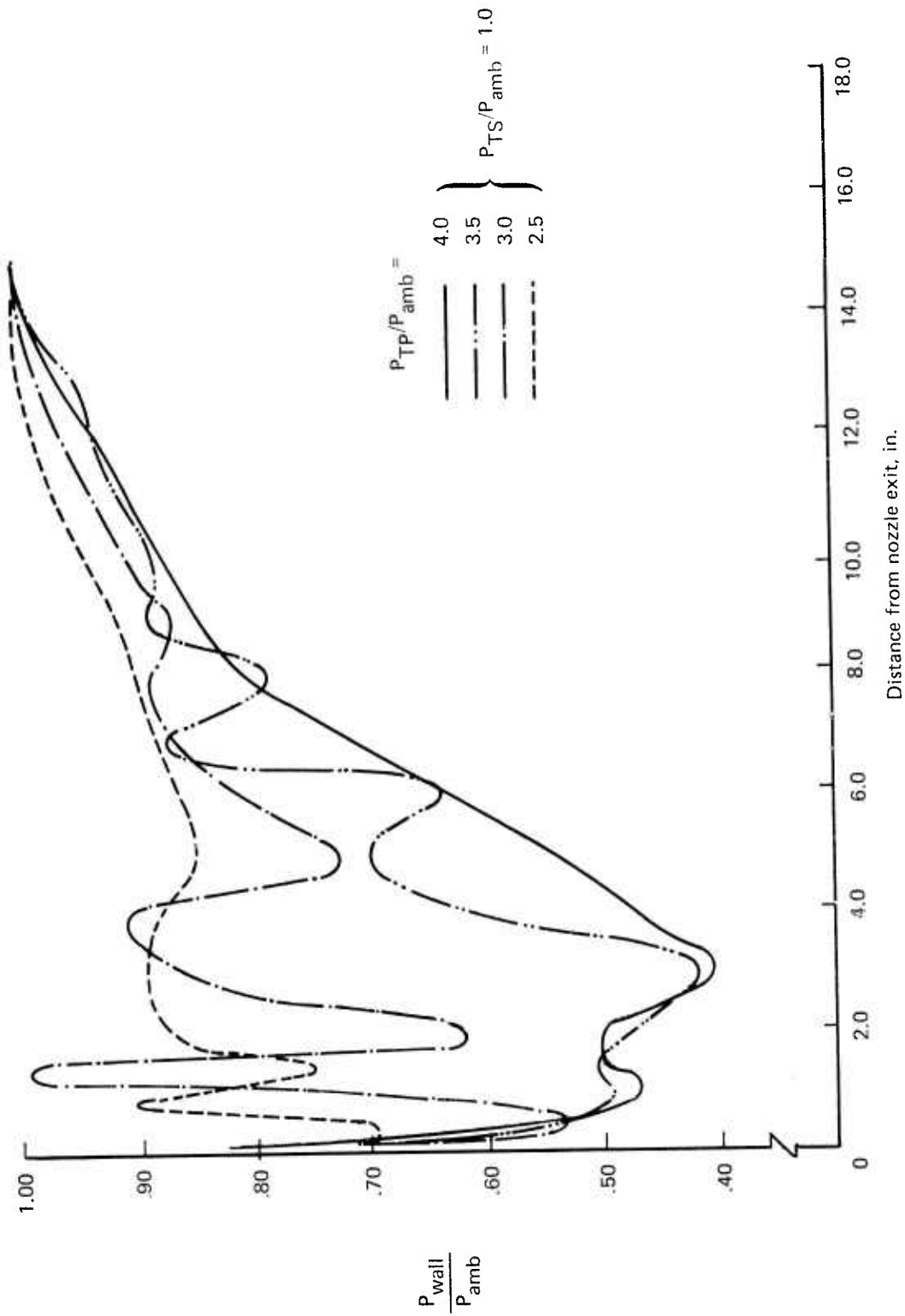


Figure 40.—Axial Static Pressure Distribution on Ejector Sidewall—Long Throat Nozzle

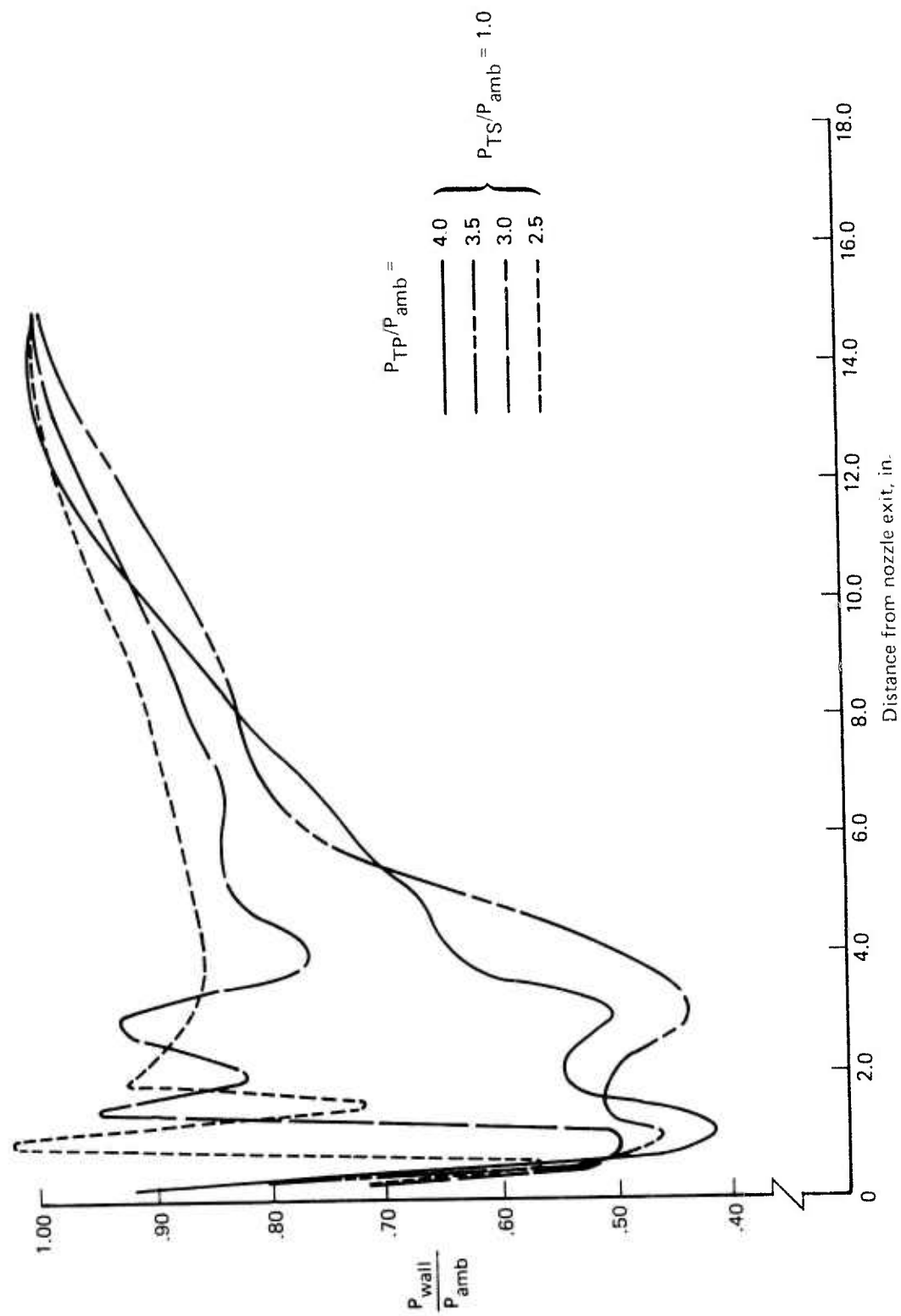


Figure 41.—Axial Static Pressure Distribution on Ejector Sidewall—Thick Base Nozzle



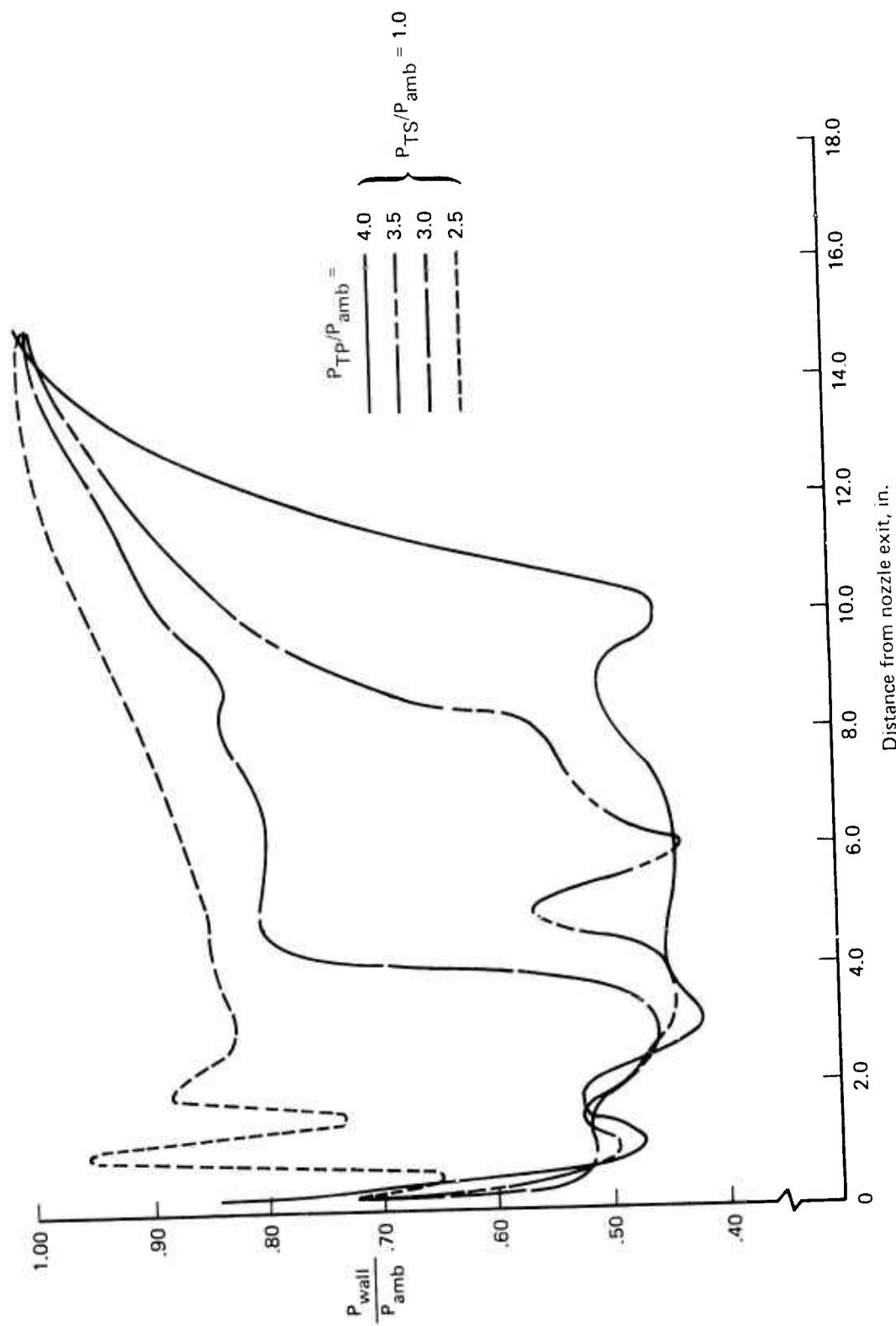


Figure 42.—Axial Static Pressure Distribution on Ejector Sidewall—High Turbulence Nozzle

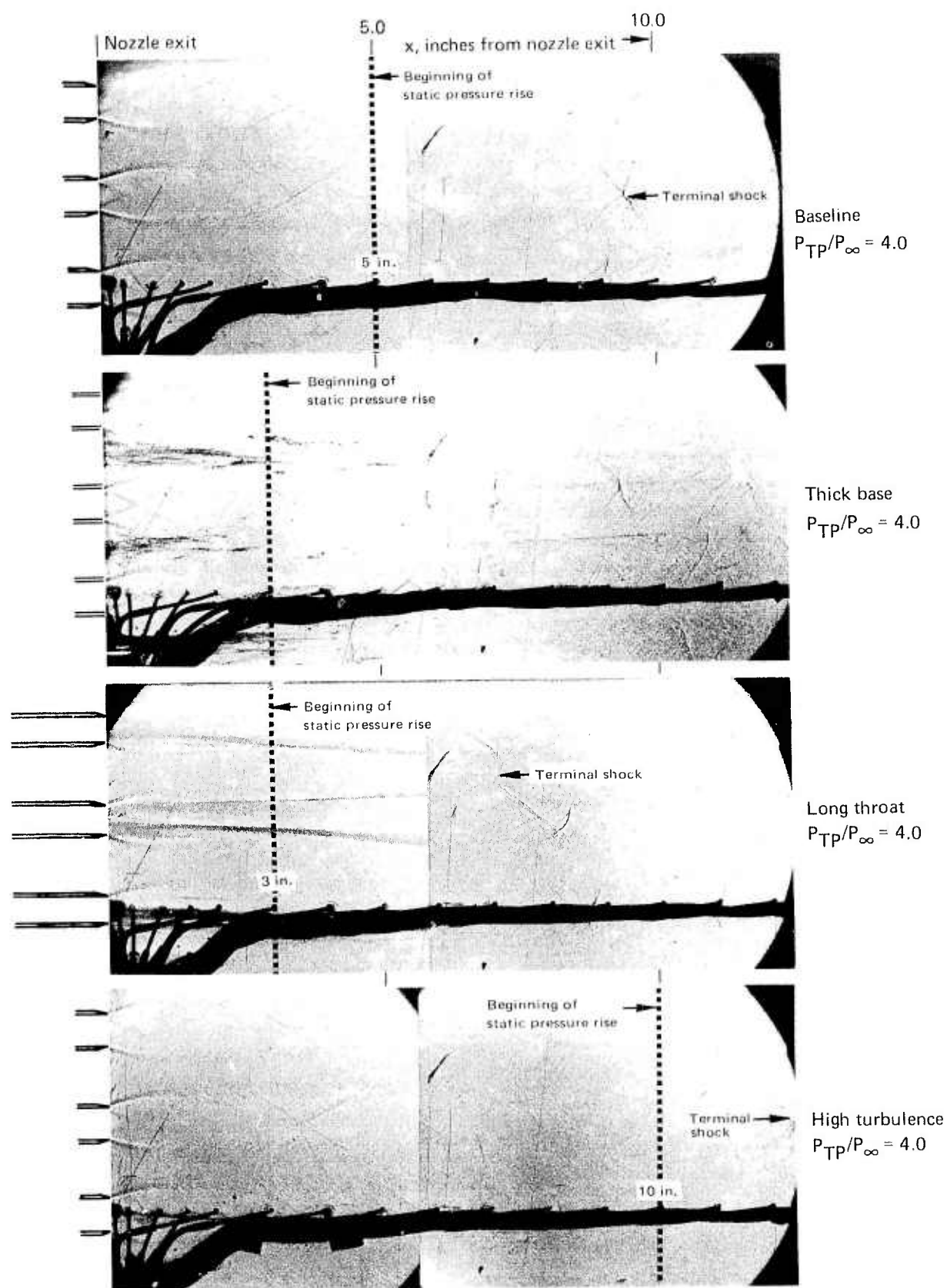


Figure 43.—Composite Shadowgraphs of Correlation of Terminal Shock Location With Static Pressure Rise,  $P_{Tp}/P_{\infty} = 4.0$

## REFERENCES

1. J. A. Ranner and D. E. Cuadra, *Velocity and Shear Profiles in the Subsonic Jet Efflux From Model Scale Sound Suppressors, Part I: Unheated Jets*, Boeing document D6-15071, vol. 1, March 1966.
2. P. Bradshaw, "The Effect of Initial Conditions on the Development of a Free Shear Layer," *Journal of Fluid Mechanics*, vol. 26, part 2, pp. 225-236, 1966.
3. A. J. Chapman and H. H. Korst, "Free Jet Boundary With Consideration of Initial Boundary Layer," *Proceedings--2nd U.S. National Congress of Applied Mechanics*, vol. 1, pp. 723-731, 1954.
4. I. Wygnanski and O. Hawaleshka, *The Effect of Upstream Velocity Profile on the Free Mixing of Jets With an Ambient Fluid*, Boeing Scientific Research Laboratories document D1-82-0528, April 1966.
5. J. F. Foss and S. J. Kleis, *Preliminary Results for a Large Angle Oblique Jet Impingement and Flow for the Effect of Initial Conditions on the Near Field of an Axisymmetric Jet*, NASA-CR-121257, May 1973.
6. Øyvind K. Oseberg and S. J. Kline, *The Near Field of a Plane Jet With Several Initial Conditions*, Stanford University, Department of Mechanical Engineering, Thermosciences Division report MD-28, May 1971.

PRECEDING PAGE BLANK NOT FILMED